Accepted Manuscript

A possible origin of intraplate earthquakes in the Kachchh rift zone, India, since the 2001 M_w7.7 Bhuj earthquake

Prantik Mandal

PII: S1367-9120(18)30421-8
DOI: https://doi.org/10.1016/j.jseaes.2018.10.006
Reference: JAES 3667

To appear in: *Journal of Asian Earth Sciences*

Received Date: 9 May 2018
Revised Date: 26 September 2018
Accepted Date: 16 October 2018

Please cite this article as: Mandal, P., A possible origin of intraplate earthquakes in the Kachchh rift zone, India, since the 2001 M_w7.7 Bhuj earthquake, *Journal of Asian Earth Sciences* (2018), doi: https://doi.org/10.1016/j.jseaes.2018.10.006

A possible origin of intraplate earthquakes in the Kachchh rift zone, India, since the 2001 M_w7.7 Bhuj earthquake

Corresponding Author:

Dr. Prantik Mandal
Chief Scientist, CSIR-NGRI,
Hyderabad-500007, India.
Email:prantikmandal62@gmail.com
Phone: +91-7893286892
Fax:+91-40-23434651

ABSTRACT

We herein use the joint inversion of P-receiver functions and fundamental mode group velocity dispersion data (9-70 s) of Rayleigh and Love waves to estimate crustal and lithospheric thicknesses at twenty three-component mobile broadband stations in Kachchh, Gujarat. Modeled Moho depths range from 35 to 43 km, while lithospheric thicknesses vary from 64 to 106 km. The main result of our modelling is the delineation of a marked crustal (~2-4 km) as well as lithospheric (~10-20 km) thinning and a 2-6% drop in Vs across the lithosphere-asthenosphere-boundary (LAB), within the Samkhiali graben (associated with gravity high) underlying the central Kachchh rift zone (KRZ), where 95% of the continued aftershock activity took place since 2001. Such a large drop in Vs could be attributed to the presence of carbonatite melts in the upper mantle. Our modeling reveals a 4 km crustal thinning below the central KRZ and a 4 km crustal thickening below the surrounding riftless regions. This kind of crustal structure is inferred to induce large flexural deviatoric stresses (~50-100 MPa) in the upper crust, thereby, these stresses in the presence of regional plate tectonic stresses can bring the Samkhiali graben below the central KRZ near to the critical stress level. While stress-transfer, meteoric water (in the upper crust), and metamorphic fluid as well volatile CO_2 flows (in the lower crust) provide the required triggering effect to the critically stressed graben structure (down to 35 km depth) for generating continued aftershock activity in the Kachchh rift zone, since 2001. We also propose that the deeper circulation of volatile CO_2 through the inferred conduit (related to the 65 Ma Deccan Plume activity) extending from lower crust down to asthenosphere plays a key role in the generation of uninterrupted occurrence of earthquakes in the Kachchh rift zone, Gujarat, India.

Key words: Receiver functions, Surface wave dispersion, Group velocity, Crust, Lithosphere, Flexural stresses.

1. Introduction

The lithosphere underlying the Mesozoic Kachhchh rift zone (KRZ), northwest India, has been significantly affected by two-phase rifting episodes (viz. 184 Ma African and 88 Ma Madagascar) and the 65 Ma Deccan volcanism (Courtillot et al., 1986; Mahony et al., 2002; Sen et al., 2009). The influence of the above tectonic episodes on the crust-mantle structure has been seen through the mapped present-day thinning of crust and lithosphere below the Kachchh rift zone (Mandal, 2016 and 2017). Also, this effect has been reflected in the Bouguer gravity anomaly map of the region, showing alternate regional gravity highs (crustal thinning) and lows (crustal thickening) (Mishra et al., 2005; Khan et al., 2016).This thinning model gets further support from the results of local earthquake tomography, surface wave dispersion and receiver function modelling studies, which have imaged crustal mafic underplating, Moho upwarping and asthenospheric thinning underlying the 2001 Bhuj earthquake region (Mandal and Pujol, 2006; Mandal, 2012). In India, topography and crustal density heterogeneities associated with the Deccan volcanic province (India) have shown to induce intraplate stresses of the order of 100 MPa (Mandal et al., 1996). Thus, the crustal stresses associated with the density heterogeneities might play a key role in generating the intraplate earthquakes in the Kachchh rift zone also.

It has been seen that the occurrences of earthquakes in the continental shelf as well as in the continental rift zones are found to be significantly influenced by flexural stresses (Stein et al., 1989; Assumpcao, 1998; Assumpco et al., 2011; Zoback and Richardson, 1996). Calais et al. (2010), based on the results of their modelling of the new Madrid seismicity, showed that these stresses associated with small loads could be of larger magnitude (~ 100 MPa) contributing significantly to intraplate stress regime. The seismicity in central Brazil is observed to be associated with large positive gravity anomalies, which has been attributed to the uncompensated lithospheric load (leading to flexural bending of the lithosphere) that resulted in large modeled compressional stresses in the upper crust (Assumpcao and Sacek, 2013). Assumpcao et al. (2016) have shown that most of the seismicity in Brazil are confined to the regions with high positive (0 to 20 mGal) gravity anomalies and fewer earthquakes have occurred in the region with low (-50 to -30 mGals) gravity anomalies. In addition, they proposed that the observed correlation between neotectonic features and epicenters in Brazil is due to stress concentration caused by intersection tectonics (Gangopadhyay and Talwani, 2007), lateral density variation (Assumpcao et al., 2004), and flexural stresses (associated with intracrustal as well as lithospheric loads) (Zoback and Richardson, 1996; Assumpcao and Sacek, 2013). Recently, Levandowski et al. (2017), based on their finite element modelling results, showed that high-gravity-derived deviatoric stresses could control the occurrence of intraplate seismicity in the North American Great Plains. Bilham et al. (2003) proposed that stresses induced by the flexural bulge of the Indian plate are playing a key role in controlling the spatial disposition of intraplate earthquakes in India. In Kachchh, the locations of moderate to large earthquakes have occurred in the lower crust below the fault zones, which are associated with large positive Bouguer gravity anomalies, indicating significant crustal thinning (Khan et al. 2017). Thus, it is apparent that the occurrence of earthquakes in Kachchh might have some causal relationship with the heterogeneous crust-mantle structure associated with the Kachchh rift zone, Gujarat, India.

The receiver function (RF) technique has been found to be very useful in delineating crust-mantle structure associated with any seismically active regions in the world (Clayton and Wiggins, 1976; Langston, 1979; Mandal, 2010). This technique has shown to model large velocity variations quite well, but it has got poor resolving power for broad velocity transitions. This observation suggests that the RF technique is more sensitive to impedance contrast rather than to absolute velocity over depth (Clayton and Wiggins, 1976; Langston, 1979). On the contrary, surface waves are sensitive to the average shear velocity contrast rather than to impedance contrast along the interfaces (Julia et al., 2000). Thus, both RF and surface wave studies should be used jointly to delineate the crustal-mantle structure in a better fashion (Ozalaybey et al.,1997; Julia et al., 2000) by reducing the lack of uniqueness of each data set and minimizing the dependence of the final result on the initial model. Earlier investigations in the KRZ revealed that crustal thicknesses vary from 33 to 46 km, through inversion of P-receiver functions (Mandal, 2010), while they range from 35 to 43 km, through joint inversion of P-RF and surface wave dispersion data (Mandal, 2012). The lithospheric thickness is found to be 70 km, from the thermal modeling (Mandal and Pandey, 2010) while they vary from 70 to 103 km, from the joint inversion of P-RF and surface wave dispersion data (Mandal, 2012). Thus, above estimates suggest a heterogeneous distribution of crustal and lithospheric thicknesses in the KRZ, however, these estimates from earlier studies suffer limitation due to few RFs, poor station coverage, and a less number of good teleseismic and regional events. This calls for the re-estimation of the crust-mantle structure using a better dataset of good teleseismic as well as regional events, and a better fundamental mode dataset of surface wave group velocity dispersion with a good resolution. Since, the seismicity in the KRZ has been monitored by our Institute during 2001-16, with a mobile seismic network of twenty three-component broadband seismographs. Thus, this network provided us with many good teleseismic events. Besides, a recent work of Mandal (2015) presented fundamental mode group velocity dispersion data of Rayleigh and Love waves (for 9-70 s) for the Kachchh region. This new broadband dataset of good teleseismic events and the well-resolved dispersion data provided us with the motivation to take a fresh initiative to delineate fine crustal and lithospheric structures associated with the KRZ. Finally, an attempt is made here to interpret our results concerning seismogenesis of intraplate earthquakes occurring in the Kachchh rift zone.

2. Geology, Gravity, Seismic network and Data

Following the breakup of Gondwanaland, a network of rifts was developed along the western margin of India (Biswas, 1987). The Kachchh rift zone, which was formed in Mesozoic, is a part of the above-mentioned network of rifts. The Geological sequence of the Kachchh region is mainly characterized by Quaternary/Tertiary sediments, Deccan volcanic rocks and Jurassic sandstones, which are resting on the Archean basement (Gupta et al., 2001). The north-dipping Nagar Parkar fault in the north and the south dipping Kathiawar fault in the south are acting as the shoulders of the Kachchh rift. The E-W trending Allah Bund fault, Island belt fault, Kachchh mainland fault and Katrol Hill fault are other major faults in Kachchh (Fig. 1).

In Kachchh, the locations of moderate to large earthquakes have occurred in the fault zones, which are associated with large Bouguer gravity anomalies (Figs. 2a-c; Khan et al. 2017; Mandal, 2016). Figs. 2a-c shows Bouguer gravity anomaly map (in mGals) of Kachchh, Gujarat, along with JHD relocations of aftershocks during 2001-06, 2007-08, 2009-10 and 2011-16, respectively. On an average, these maps show regional gravity highs (+2 to +20 mgals) over the central Kachchh rift zone and surrounding uplifted areas except the region south-west of it, which is characterized by the significant Bouguer gravity lows of -8 to -20 mgals (Figs. 2a-c). The observed alternate pattern of gravity highs and lows might be indicating the presence of a series of graben and horst structures in the Kachchch rift zone (Khan et al., 2017).

The data used in this paper correspond to digital waveforms of teleseismic earthquakes recorded at twenty mobile broadband seismographs of the Kachchh seismic network of the National Geophysical Research Institute (NGRI), Hyderabad, India, during February 2001 – December 2016 (Fig. 1a). Each seismograph station is equipped with a 24-bit REFTEK digital recorder and 3-component broadband (natural period 30 – 120 seconds) Guralp sensor for recording local, regional and teleseismic events. The data are recorded in continuous mode with a sampling rate of 100/50 samples/s. Most of these stations are located on hard sediments or rocks [Jurassic sediments or basalt]. However, a few of these stations are on a thin soil layer.

3. Methodology

3.1 *Analysis of RF*

For our study, we select the best quality digital waveforms of 241 good teleseismic events of $M_w \geq 6.0$ having a large signal-to-noise ratios and clear P-arrivals (with back azimuth between

30° and 310°, epicenters between 30°S and 90°N, and ray parameters ranging from 0.040 to 0.080 s/km) (Fig. 1b). First, we select a 120 s long windowed broadband waveforms starting 10 s before the P-wave arrival. Next, these windowed waveforms are detrended, tapered, and decimated to a uniform sampling rate of 10 samples per second. Then, a band-pass (0.05–8 Hz) filter is used to avoid aliasing and low-frequency instrumental noise. Finally, the resulting horizontal components are rotated around the vertical component for computing the corresponding radial and transverse traces. The radial and transverse RFs are estimated from the three-component digital waveforms using the iterative time domain deconvolution procedure of Ligorria and Ammon (1999) with 200 iterations. In the time domain deconvolution, the frequency content of the RF is controlled by the Gaussian filter parameter 'a'. For studying detailed crust-mantle structure, two frequency bands corresponding Gaussian width factors, $a = 1.0$ ($f < 0.5$ Hz) and $a = 2.5$ ($f < 1.25$ Hz), are considered for estimating RFs for each event. These provide better control in delineating velocity interfaces through helping in discriminating rapid changes in seismic velocities at gradational transitions (Owens and Zandt, 1985; Julia, 2007). Finally, those deconvolutions that reproduced less than 85% of the signal energy on the radial component (when convolved back with the vertical trace) are discarded. For this study, we use a total of 452 RFs from 20 broadband stations, out of 6000 waveforms. Also, a move-out correction is applied to individual receiver functions, to enhance the conversions from deeper interfaces, using the inbuilt utility of RFTN program of Hermann's seismological software (Herrmann, 2004).

To illustrate details of the RF analysis procedure, we discuss here the analysis of broadband data from 20 broadband stations (Fig. 1a). First, we study all individual radial RFs from all twenty stations as a function of horizontal slowness ranging from 0.04 to 0.08 s/km and back azimuth varying from 30^o to 310^o. In general, the radial RFs show clear P-to-S conversions (P_{ms} at 4.6-5.8 s after P_p [i.e., direct P arrival], Fig. 3) and some weak multiples (i.e., P_pP_{ms} and P_pS_{ms}+P_sP_{ms}) from the crust–mantle boundary, suggesting probably a clear Moho underlying the study region. They also show a clear positive conversion (P_{cs}) from some upper crustal interface at 2-2.5 s after P_p and an apparent negative arrival at 11–14 s after P_p, associated with the P-to-S conversion (P_{ls}) from the lithosphere–asthenosphere boundary (LAB) (Fig. 3). We notice that prominent P_{ss}, P_{ms} and P_{ls} characterize all individual radial RFs from all 20 broadband stations while some weak Moho multiples are also seen in all individual radial RFs (Fig. 3). Finally, these individual radial RFs are used as input for the inversion modeling of radial RFs for different back azimuths, which is discussed hereunder.

After estimating the radial and transverse RFs from the time domain deconvolution of Ligorria and Ammon (1999), first, we cut the radial RFs from -5 to 20 s for modeling crustal and lithospheric structure through the inversion modeling. The available velocity models down to a depth of 140 km, which have been obtained using the inversion of P-RFs (Mandal, 2016), are used for this study. Finally, we select 452 radial RFs from twenty broadband stations with all of the high-quality waveforms are in this set. A time window (from -5 s (before the P-arrival) to 20 s (after the P arrival)) is used to calculate radial RFs for the joint inversion modeling of P-RFs and surface wave dispersion data, which will include both the main Ps conversions and all the principal multiples relevant to crustal and lithospheric structure (Figs. 3-13a,b), which is discussed hereunder.

3.2 *Surface Wave Group Velocity Dispersion (SWD) Measurements*

Here we use the Rayleigh and Love wave group velocity dispersion measurements, which are obtained through the FTAN analysis of broadband data of nine regional earthquakes from a total of 20 stations in the continental region of India (Mandal, 2015). This surface wave study was done using data from 20 three-component broadband stations deployed in the continental region of India, which samples the Indian continent very well (Fig. 4a). A detailed description of the FTAN is given by Levshin et al. (1992), and papers referred to therein. Mandal (2015) used a stacking technique in the frequency-time domain to measure fundamental mode group velocities of Rayleigh and Love waves and corrected large errors at long periods using the procedure of Shapiro and Singh (1999) (Dziewonski et al., 1969; Campillo et al., 1996; Shapiro et al.,1997). The average dispersion curves (Figs. 4b and c) were estimated by Mandal (2015), using a logarithmic stacking in the period-group velocity domain. The details can be seen from Mandal (2015) and Singh et al. (1999). These figures suggest a stable dispersion curve from 9 to 70 s, which are used here to perform the joint inversion of P-RFs and surface wave dispersion data. Surface wave dispersion data within this range can be used to delineate the shear velocity structure up to a depth of 200 km (Hermann, 2004; Singh et al., 1999; Pasyanos, 2010; Mandal, 2015).

The final average group velocity dispersion curves along with standard deviations for the study region (Figs. 4b,c) show a stable group velocity dispersion for both Rayleigh and Love waves over a period of 9-70 s. The maximum errors of 0.3-0.5 km/s are obtained for the longer period (50–70 s) for both Rayleigh- and Love-wave group velocity dispersion curves (Mandal, 2015). The group velocities of Rayleigh waves in Kachchh (Fig. 4a) suggest (i) a subdued change from 2.80 to 2.95 km/sec at 9-20 s, (ii) a gradual increase from 2.95 to 3.60 km/s at 20-43 s, and (iii) a gradual decrease from 3.60 to 3.52 km/s at 43-70 s. The group velocities of Love waves in Kachchh (Fig. 2b) suggest (i) a gradual increase in group velocity from 3.10 to 3.32 km/sec at 9-20 s, (ii) a steep increase in velocities from 3.32 to 3.70 km/sec at 20-42 s, (iii) a gradual decrease in velocities from 3.70 to 3.62 km/s at 42-54 s, and (iii) a steep increase in group velocities from 3.62 to 3.90 km/s at longer period of 54-70 sec.

3.3 *Joint Inversion of RFs and Group velocity dispersion data*

The assumption of a plane-layered structure leads to a non-uniqueness problem for the inversion of both receiver functions and surface wave group velocity dispersion data. RF cannot provide unique absolute velocity information while surface group velocity dispersion cannot identify discontinuities uniquely. Due to this fact, these two different data sets are merged into one inversion scheme, through performing a joint inversion for velocity structure. We combined the group velocities of fundamental mode surface waves with the radial P-receiver functions. We adopted the method of Julia et al. (2000), based on an iterative damped least-squares scheme. This method, then, provides an easy way to control trade-offs between fitting the receiver functions and the dispersion curves (normalised by the data uncertainty and some points). This method also compromises between model smoothness and data fitting. After running a suite of inversions, weighting parameters and the smoothness are determined using empirical relations. A detailed description of the method could be seen from Julia et al. (2000).

The joint inversion of radial P-RFs (for a=1.0 (f<0.5 Hz), as well as a=2.5 (f<1.25 Hz)) and fundamental group velocity dispersion data for Rayleigh and Love waves, are performed using Julia et al. (2000). We selected those 580 P-receiver functions (over different back-azimuth / horizontal slowness values) with all of the high-quality waveforms that are in this set. For the joint inversion study, we also use average fundamental mode group velocity dispersion data for Kachchh (Figs. 4b,c). Due to the uneven azimuthal distribution of teleseismic events (Fig. 1b), reliable anisotropic structures are difficult to retrieve with this data set. For our study, we use joint inversion code of P-RF and SWD data inbuilt in the joint96 seismological code of Herrmann (2004) that utilizes the Julia et al. (2000)'s joint inversion technique to delineate 1-D shear velocity structure.

For joint inversion study, we use the velocity models down to a depth of 200 km for twenty 3-component broadband seismograph stations in Kachchh, which are estimated earlier by the inversion of P-RFs (Mandal, 2017). The Moho depths for the initial models are varying from 33 (at MND) to 46 (at KNM) km. The details can be found in Mandal (2017). Initial velocity models consist of the thickness, V_p, V_s, density (ρ), Q_p and Q_s, of each layer. For joint inversion, a fixed value of 1.73 is considered for each layer. And, V_s and layer thicknesses are chosen to be the unknown model parameters. This inversion scheme iteratively inverts for the S-wave velocity and then calculates the P-velocity using the V_p/V_s ratio of the initial model. Subsequently, the new density is computed from the new V_p using the relation of Berteusen (1977). Then, the number of layers is determined from the prior knowledge of crustal structure. After determining the number of layers, V_s, and thickness, of each layer, are adjusted within specified ranges to fit observed receiver functions. Several iterations are needed because inversions starting with models that do not predict group velocity data well, do not converge. Joint inversions are repeated for each iteration to find joint models that fit the receiver functions (Figs. 5-9) and Rayleigh as well as Love waves group velocity dispersion data (Figs. S1-S4, Appendix A). For different stations, the inversion scheme provided a stable solution after 30 iterations. Thus, here we perform 30 iterations of inversion to obtain the final model. Therefore, 30 different velocity models for 30 iterations are obtained from the joint inversion at each station, which are shown by different shades of red, green and blue as shown in Figs. 9-13a. And, the initial and final shear velocity models are shown by thick grey and black lines, respectively (Figs. 9-13). When we ran the joint inversion, we can fit the surface waves without significantly degrading the fit to the receiver functions. The joint inversion continues until we get the best-fit Vs model showing good correlation (85%) between the all available observed and inverted P-RFs (over the available range of horizontal slowness and back-azimuths at one station) and fundamental mode SWD data of Rayleigh and Love waves. The same procedure of joint inversion is performed to estimate the best-fit 1-D shear velocity model for all twenty broadband stations (down to a depth of 200 km) in the Kachchh rift zone (Figs. 9-13). The inverted crustal and lithospheric models from the joint inversion study for all the twenty sites are shown in Figs. 9-13. The contour plots of estimated Moho depths (M), and lithospheric thicknesses (L) are shown in Figs. 13c-d (Table 1).

4. Results and Discussions

The joint inversion of P-RF and fundamental mode group velocity dispersion data for both Rayleigh and Love waves at twenty broadband sites provide new constraints on the basement, crustal and lithospheric structure of the Kachchh rift zone (KRZ) (Figs. 9-13). The results for crustal structure and lithospheric thicknesses in the KRZ are listed in Table 1.

Figs. 2a-c shows Bouguer gravity anomaly map (in mGals) of Kachchh, Gujarat, along with Joint Hypocentral Determination (JHD) relocations of aftershocks during 2001-06, 2007-08, 2009-10 and 2011-16, respectively. We can notice that very consistently most of the earthquakes have occurred within the Samkhiali graben, during 2001-16, which is associated with gravity high (0-20 mgal). Few earthquakes have also occurred in the adjacent horst structure associated with gravity low (-8 to -20 mgal). The confinement of the continued aftershock activity associated with the Samkhiali graben (gravity high) could be attributed to the seismic failure due to the presence of sizable intraplate stresses associated with a marked crustal thinning (crustal density heterogeneities), below the central Kachchh rift zone.

Here, we consider those depths as the Moho depths where we obtained a shear velocity exceeding 4.1 km/s, while lithospheric depths are considered to be associated with a marked drop in Vs (exceeding 2%). The estimated crustal thicknesses range from 35 km (at KNP and MND) to 43 km (at KNM, SIV, MTP, GDD, JUM, KVD, BHU, NPR, VND and TPM), with a mean crustal thickness of (38±2) km in CKRZ while they vary from 41 to 43 km in the surrounding riftless regions (Table 1). On an average, the crust below the CKRZ is found to be thinner in comparison to that below the surrounding riftless regions (Table 1; Fig. 13c). The estimated lithospheric thicknesses vary from 64 (at BHA) to 106 (at NDD) km below the CKRZ. We notice a significant lithospheric thinning of 10-15 km beneath the main rupture zone (an area of 40 km x 40 km) of the 2001 Bhuj mainshock that correlates well spatially with the location of Samkhiali graben (SG) (Fig. 14). This lithospheric thinning model gets further support from the modeled large negative travel-time residuals in the CKRZ (Figs. 13c,d; Mandal, 2017). Note that the continued aftershock activity during 2001-16 has also been found to be confined below the SG in CKRZ, which characterized by large positive Bouguer gravity anomalies of the order of 2-20 mgals. The smaller mean lithospheric thicknesses of the order of 84-88 km are obtained below the CKRZ and the regions north and east of it, where large positive regional Bouguer gravity anomalies are also reported (Figs. 2a-c). The larger mean lithospheric thickness of the order of 93 km is estimated below the riftless surrounding regions southwest of CKRZ, where large negative Bouguer gravity anomalies (-8 to -20 mgals) are seen (Figs. 2a-c). On an average, the lithosphere below the region is found to be dipping from north to southwest (Table 1). The lithosphere underlying the SG in the CKRZ is found to be heterogeneous with a marked lithospheric undulation of 10-20 km, which can contribute sizable crustal stresses associated with the SG.

We observe a marked reduction in shear velocity (2.4-5.8%) at the lithosphere-asthenosphere boundary below the KRZ suggests the presence of carbonatite partial melts in the asthenosphere (Figs. 9-13; Mandal, 2016). These partial melts could be representing the imprints of earlier magmatism episodes viz. syn-rift and 65 Ma Deccan volcanism episodes (Kennet and

Widiyantoro, 1999). We observe a marked drop (2.4-5.8%, with a mean drop of 4.0%) in Vs below the central KRZ, which is also characterized by a marked crustal as well as lithospheric thinning, and a positive Bouguer gravity anomaly (Figs. 13c-d and 14a; Table 1). Our modeling results show that a significant reduction of 5.8% in Vs in the upper mantle is noticed below NDD site where the thinnest crust (~35 km) is also obtained. However, a 35 km crust is also obtained at MND coastal station, where, the Vs drop in upper mantle is also found to be maximum (~7.2%). The region below VND station with a thick crust of 43 km is noticed to be associated with a small drop of 2.2% in Vs in the upper mantle, which could be attributed to its locations away from the KRZ. Note that the maximum mean drop in Vs of 4.3% is found at stations in the region north of the CKRZ (Table 1), which could be related to their location near to the Kaladungar where mantle xenoliths are found. These stations are also observed to be associated with a large positive regional gravity high and a thin lithosphere of 84±7 km thickness (Table 1). Two (BHU and NGR) out of five stations in the south-west of CKRZ show a larger drop of 4.8% in Vs in the upper mantle, which could be attributed to their spatial locations near to the CKRZ and exposed Deccan basalts (Fig. 1a). While a smaller drop (~3.5-3.6%) in Vs is noticed in the upper mantle underlying the remaining three stations in the south-west of CKRZ. A Larger drop of 5.5 % in Vs is also obtained in the upper mantle underlying the KNM station, which is found to be associated with a relatively thin lithosphere (~78 km). While SIV station is found to be associated with a smaller drop of 3.5% in Vs in the upper mantle, which is located on a Mesozoic hillock of the Wagad uplift (Fig. 1a).

Note that the finite element visco-elastic modeling of flexural intraplate stresses associated with crustal density heterogeneities in the central Brazil has shown to induce large compressional stresses of the order of 50-100 MPa in the upper crust just above the density load at crust-mantle boundary, due to the high density shallower mantle rocks in the area of thin crust (Assumpcao and Sacek, 2013). In the Kachchh rift zone, we notice that a 41–43 km thick crust is seen in the west while a ~43 km thick crust in the east (at SIV, VND and KNM stations, accompanied by elevated topography and low Bouguer gravity) (Figs. 1a, 2a-c; Table 1). While a thinner crust (~35-39 km) in the middle (central KRZ) (an area of low elevation and high gravity) coincides with the Kachchh seismic zone. We also found a 42-43 km thick crust in north and south of the central KRZ. Thus, we infer that a 4 km crustal thinning below the central KRZ (Samkhiali graben) and 4 km crustal thickening below the surrounding riftless regions of it, can give rise to a 2-D crustal model similar to the crustal model of Central Brazil as considered by Assumpcao and Sacek (2013) for their viscoelastic finite element modeling. Assumpcao and Sacek (2013) showed that this kind of crustal structure could induce large flexural stresses (associated crustal density anomaly) of the order of 50-100 MPa. Therefore, similar large flexural stresses could be possible to be generated in the upper crust by our modeled crustal structure of the KRZ. These large stresses in the presence of regional plate tectonic stresses (probably caused by the ridge push (Mandal et al., 1996)) might be bringing the graben structure near to the critical stress level, where 95% of the aftershock activity is occurring since the occurrence of the 2001 Bhuj mainshock. This critically stressed Samkhiali graben (bounded by KMF in the north and NWF in the south) is probably releasing energy (in the form of continued occurrences of intraplate earthquakes) due to small stress perturbations in the stress regime resulting from the stress-transfer and meteoric water (at 0-10 km depth) or metamorphic fluid as well as volatile CO_2 (at 10-35 km depth).

The contour plot of filtered residual Bouguer gravity anomaly (using a high-pass filter with a cutoff wavelength of 375 km) (Khan et al., 2017) along with the JHD relocated Kachchh seismicity during 2001-2013 is shown in Fig. 14a. On an average, the map shows regional gravity highs (+2 to +20 mgals) over the central Kachchh rift zone and surrounding uplifted areas except for the region south-west of it, which is characterized by the significant Bouguer gravity lows of -8 to -20 mgals (Fig. 14a). The observed alternate pattern of gravity highs and lows might be indicating the presence of a series of graben and horst structures in the Kachchch rift zone (Khan et al., 2017). This figure shows that 95% of the continued aftershock activity is occurring within the Samkhiali graben (gravity high, shown by AB blue solid line), below the central Kachchh rift zone while fewer events took place in the neighboring low Bouguer gravity anomaly (horst structure) (Fig. 14a).

In Fig.14b, we propose a schematic tectonic model to explain the seismogenesis of earthquakes occurring in the KRZ since the occurrence of the 2001 M_w7.7 Bhuj mainshock. This figure shows an NE-SW tectonic cross-section showing all major tectonic features/faults in the KRZ including tectonic faults, horst and half-grabens. The AB line marks the Samkhiali graben structure (extending from KMF to NWF) in Fig.14a,b, which is found to be characterized by gravity high and a marked concentration of aftershock activity of the 2001 Bhuj earthquake. Fig. 14b also shows hypocentral locations of the 2001 mainshock and major M5 aftershocks, which are lying along the NWF and within the lower crustal mafic intrusive, except one M5 event that occurred on the GF. Figs. 2a-c, 14a show the JHD locations of the aftershocks during 2001-13, suggesting the main concentration of aftershock activity within the Samkhiali graben. Our modeling delineates a crustal thinning of 4 km and a lithospheric thinning of 10-20 km underlying the Samkhiali graben in the central KRZ as shown in Fig.14b, which, in turn, enabled us to infer a southward inclined conduit (extending from lower-crust down to asthenosphere) for the deeper circulation of volatile CO_2emanating from the carbonatite melts in the asthenosphere. Note that carbonatite melt would travel upward depending on the P-T condition in the upper mantle and it would crystallize while crossing the thermal LAB (at 70 km depth (Sen et al., 2009; Mandal and Pandey, 2010). During the crystallization process, it would release the volatile CO_2, which would then travel to lower-crust through the inferred conduit (Fig. 14b). This deeper circulation would result in the presence of entrapped volatile CO_2 in the lower crust, which probably provides the triggering effect for generating uninterrupted occurrence of earthquakes within the Samkhiali graben in the KRZ for last 17 years. The local earthquake tomography images an 18-km thick mafic under-plated layer (at 24-42 km depths) underlying the SG, which has resulted in a sub-crustal high-velocity eclogitic layer beneath the region (Mandal and Pandey, 2010). This kind of crustal structure along-with a marked crustal thinning would contribute sizable crustal stresses associated with the Samkhiali graben. Additionally, a 10-20 km lithospheric thinning below the SG would also contribute additional crustal stresses. This crustal stress-state would bring the Samkhiali graben near to critical stress level and then a small stress perturbation due to stress transfer, or fluid flow mechanisms would lead to uninterrupted seismic failure, thereby, the continued aftershock activity at Kachchh, Gujarat.

5. **Conclusions**

The joint inversion of P-RF and fundamental mode group velocity dispersion data of Rayleigh and Love waves led to following new insights on the Geodynamic processes acting in the Kachchh rift zone (KRZ).

i. Modeled moho depths in KRZ range from 35 to 43 km while lithospheric thicknesses vary from 64 to 106 km.

ii. The central KRZ occupying Samkhiali graben is characterized by a marked 4 km crustal thinning as well as lithospheric thinning (~10-20 km) and a 2-6% drop in V_s across the lithosphere-asthenosphere-boundary (LAB), which could be attributed to the magmatism associated with the Deccan mantle plume and syn-rift volcanism episodes.

iii. The surrounding riftless regions are found to be characterized by crustal thickening.

iv. The regions in north and east of the central KRZ are found to be characterized by lithospheric thinning while the regions in the southwest of the central KRZ are observed to be characterized by lithospheric thickening.

v. Overall, an increasing lithospheric thickness from north to the southwest is noticed over the region.

vi. The observed marked reduction of shear velocity (2.4-5.8%) across the lithosphere-asthenosphere boundary (LAB) below the KRZ suggests the presence of patches of carbonatite melts in the asthenosphere, evidencing the imprints of earlier magmatism episodes viz. syn-rift and Deccan volcanism.

vii. Most interestingly, zones with regional gravity highs in the CKRZ and the regions north and east of it are modelled to be characterized by lithospheric thinning while zones with regional gravity lows in southwest of the CKRZ are found to be characterized by lithospheric thickening.

viii. We also notice that large to moderate size earthquakes in Kachchh, India, have occurred in the fault zones associated with large positive Bouguer gravity anomalies. This observation suggests that flexural deviatoric stresses related to crustal mass/density heterogeneities play a crucial role in the generation of intraplate crustal earthquakes in the Kachchh rift zone, India.

ix. We also infer that a 4 km crustal thinning below the central KRZ and 4 km crustal thickening below the surrounding regions of it, as revealed by our modeling, could induce compressional flexural stresses of the order of 50-100 MPa in the upper crust, thereby, continued occurrences of crustal intraplate earthquakes in the Kachchh rift zone.

x. We propose that large stresses associated with crustal (thinning) density anomalies and mafic intrusive bodies in the presence of regional plate tectonic stresses brought the stress regime associated with the Samkhiali graben structure (extending down to 35 km depth) near to critical stress level while stress transfer and meteoric water (in the upper crust at 0-10 km depth) or metamorphic fluid, as well as volatile CO_2 flows (in the lower crust at 10-35 km depth) provide the required triggering effect to the critically stressed graben structure for generating continued aftershock activity in the Kachchh rift zone, since 2001.

xi. We also propose that the deeper circulation of volatile CO_2 through the inferred conduit (related to the 65 Ma Deccan Plume activity) extending from lower crust down to asthenosphere plays a key role in the generation of uninterrupted occurrence of earthquakes in the Kachchh rift zone, Gujarat, India.

Acknowledgements

Author is grateful to the Director, NGRI, Hyderabad, for his kind permission to publish this work. This study is supported by the Council of Scientific and Industrial Research (CSIR) twelfth five-year plan project (HEART) at the CSIR-National Geophysical Research Institute, Hyderabad. Seismograms used in this study were recorded on twenty three-component mobile seismograph stations of a local seismic network of the Council of Scientific and Industrial Research National Geophysical Research Institute (CSIR-NGRI), Hyderabad, in the Eastern Indian shield, India. Data can be obtained through a request to the Director, Council of Scientific and Industrial Research-National Geophysical Research Institute, Hyderabad 500007, Telangana State, India (director@ngri.res.in).

References

Acton, C.E., Pristley, K., Gaur, V.K., Rai, S.S., 2010. Group velocity tomography of the Indo-Eurasian collision zone. Journal of Geophysical Research (Solid-Earth)115, B12335, 8-16.

Assumpcao, M., 1998. Seismicity and stresses in the Brazillian passive margin. Bulletin of the Seismological Society of America 78(1), 160-169.

Assumpco, M., Dourado, J.C., Ribotta, L.C., et al., 2011. The Sao Vicente earthquake of April 2008 and seismicity in the continental shelf off SE Brazil : further evidence for flexural stresses. Geophysical Journal International, doi:10.1111/j.1365-246X.2011.05198.x.

Assumpcao, M. &Sacek, V., 2013.Intra-plate seismicity and flexural stresses in central Brazil. Geophysical Research Letters 40, 1-5.

Assumpcao, M., Ferreira, J., Barros, L., Bezerra, H., Franga, G.S., Barbosa, J.R., Menezes, E., Ribotta, L. C., Pirchiner, M., Nacsimento, A.D. & Dourado, J.C., 2016. Intraplate Seismicity in Brazil. In: "IntraplateEarthqukaes" edited by Talwani, P., Cambridge University Press, 50-71.

Berteusen, K. A., 1977. Moho depth determinations based on spectral-ratio analysis of NORSAR long-period P waves. Phys.Earth Planet.Int.31, 13–27, doi10.1016/0031-9201(77)90006-1.

Bilham, R., Bendick, R., Wallace, K., 2003. Flexure of the Indian plate and intraplate earthquakes. Journal of Earth System Sciences112, 315-329.

Biswas, S.K., 1987. Regional framework, structure and evolution of the western marginal basins of India. Tectonophysics 135, 302-327.

Biswas, S. K., 2005. A review of structure and tectonics of Kutch basin, western India, with special reference to earthquakes. Current Science 88, 1592–1600.

Calais, E., Freed. A. M., Van Arsdale, R., Stein, S., 2010. Triggering of New Madrid seismicity by late-Pleistocene erosion. Nature 466, 608–611.

Chopra, S., K.M. Rao, Rastogi, B.K., 2010. Estimation of sedimentary thickness in Kachchhbasin, Gujarat Using Sp converted Phase. Pure and Applied Geophysics 167, 1247-1257.

Courtillot, V., Besse, J., Vandamme, D., Montigny, R., Jaeger, J.J., Cappetta, H., 1986. Deccan flood basalts at the Cretaceous/Tertiary boundary?. Ear.Planet. Sci. Lett. 80, 361-374.

Gangopadhyay, A., Talwani, P., 2003.Symptomatic Features of Intraplate Earthquakes. Seis. Res. Lett. 74, 863-883.

Gupta, H. K., Harinarayana, T., Kousalya, M., Mishra, D.C., Mohan, I., Purnachandra Rao, N., Raju, P.S, Rastogi, B.K., Reddy, P.R. & Sarkar, D., 2001.Bhuj earthquake of 26 January 2001. J. Geol. Soc. Ind. 57, 275–278.

Herrmann, R.B., 2004. Computer Programs in Seismology, Department of Earth and Atmospheric Sciences, St. Louis University, St. Louis, Missouri, USA.

Julia, J., Ammon, C.J., Herrmann, R.B., Correig, A.M., 2000. Joint inversion of receiver function and surface-wave dispersion observations. Geophys. J. Int. 143, 99–112, doi10.1046/j.1365-246x.2000.00217.x.

Kennett, B.L.N., Widiyantoro, S., 1999. A low seismic wave-speed anomaly beneath northwestern India: a seismic signature of the Deccan Plume?. Earth Planet Sci. Lett. 165, 145-155.

Khan, P.K., Mohanty, S.P., Sinha, S., Singh, D., 2016. Occurrences of large-magnitude earthquakes in the Kachchh region, Gujarat, western India: Tectonic implications. Tectonophysics 679, 102–116.

Ligorria, J. P., Ammon, C. J., 1999. Iterative deconvolution and receiver function estimation. Bull. Seismo. Soc. Am. 89, 1395–1400.

Mahoney, J. J., Duncan, R.A, Khan, W., Gnos, E.,McCormick, G.R. 2002. Cretaceous volcanic rocks of the South Tethyan suture zone, Pakistan: Implications for the Réunion hotspot and Deccan Traps. Earth Planet. Sci. Lett. 203, 295–310.

Mandal, P., 2007. Sediment Thicknesses and Qs vs. Qp relations in the Kachchh rift basin, Gujarat, India using Spconverted phases. Pure Appl. Geophy. 164, 135-160.

Mandal, P., 2016. Variations of seismic velocities in the Kachchh rift zone, Gujarat, India, during 2001–2013. Tectonophysics 672/673, 68-86, DOI:10.1016/j.tecto.2016.01.040.

Mandal, P., 2017. Influence of Deccan Volcanism and Synrift magmatism on the crust-mantle structure and its implications toward the seismogenesis of earthquakes occurring in the Kachchh rift zone, In a special volume of "Tectonics of the Deccan Large Igneous Province" by Mukherjee, S., Misra, A. A., Calve `s, G. &Nemc ˇok, M. (eds) 2017. Tectonics of the Deccan Large Igneous Province. Geological Society, London, Special Publications 445, 189–218.

Mandal P., Pujol, J., 2006. Seismic Imaging of the Aftershock Zone of the 2001 Mw 7.7 Bhuj Earthquake, India. Geophysical Research Letters 33, L05309, 1-4. doi:10.1029/2005GL025275.

Mandal, P., 2012.Passive source seismic imaging of the crust and upper mantle beneath the 2001 Mw7.7 Bhuj earthquake region, Gujarat, India. Bulletin of Seismological Society of America 102(1), 252-266.

Mandal, P., Manglik, A., Singh, R.N., 1996.Intraplate stress distribution induced by topography and crustal density inhomogeneities beneath the Killari, India, region. Jou. Geophys. Res. 102, 11,719-11,729.

Mandal, P., Pandey, O.P., 2010.Relocation of aftershocks of the 2001 Bhuj earthquake: A new insight into seismotectonics of the Kachchh seismic zone, Gujarat, India. Journal of Geodynamics 49, 254-260.

Mandal, P., 2011.Crustal and lithospheric thinning beneath the seismogenic Kachchh rift zone, Gujarat (India): Its implications toward the generation of the 2001 Bhuj earthquake sequence. Journal of Asian Earth-sciences 40, 150-161.

Mishra, D.C., Chandrasekhar, D.V., Singh, B., 2005. Tectonics and crustal structures related to Bhuj earthquake of January 26, 2001: based on gravity and magnetic surveys constrained from seismic and seismological studies. Tectonophysics 396, 195–207.

Pasyanos, M. E., 2010. Lithospheric thickness modeled from long-period surface wave dispersion. Tectonophysics 481, 38-50.

Owens, T. J., Zandt, G., 1985. The response of the continental crust-mantle boundary observed on broadband teleseismic receiver functions. J. Geophys. Res. 12, 705–708.

Rudnik, R.L., Fountain, D.M., 1995. Nature and composition of the continental crust: a lower crustal perspective. Reviews of Geophysics 33, 267–309.

Sen, G., Bizimis, M., Das, R., Paul, D.K., Ray, A., Biswas, S., 2009. Deccan plume, lithospheric rifting, and volcanism in Kutch, India. Earth Planet. Sci. Lett. 277, 101–111.

Sen, G., 2001. Generation of Deccan Trap magmas. Proc. Indian Acad. Sci. (Earth Planet.Sci.) 110, 409–431.

Singh, S. K., Dattatrayam, R. S., Shapiro, N. M., Mandal, P., Pacheco, J. F., Midha, R. K., 1999. Crustal and upper mantle structure of Peninsular India and source parameters of the May 21, 1997, Jabalpur earthquake [Mw 5.8]: Results from a new regional broad-band network. Bull.Seismol. Soc. Am. 89, 1632–1641.

Singh, B., Gupta, A., Mandal, P., 2017. Sediment thicknesses and Q_s-Q_p relations in the Kachchh rift basin, Gujarat, India, using converted phases. Bull. Seismol. Soc. Am. 107(5), 2532-2539.

Stein, S., Liu, M., Calais, E.,Qingsong, L., 2009. Mid-continent earthquakes as a complex system. Seism. Res. Lett. 80, 551–553.

Tewari, H.C., Surya Prakasa Rao, G., Rajendra Prasad, B., 2009. Uplifted crust in parts of western India. J. Geol. Soc. India, 73, 479–488.

Zoback, M. L., Richardson, R. M., 1996. Stress perturbation associated with the Amazonas and other ancient continental rifts. Journal of Geophysical Research 101, 5459–5475.

Figure Captions:

Figure 1: (a) Elevation (in m) map showing station distribution in Kachchh, Gujarat. Open black triangles mark the broadband seismograph stations (SIV, Sivlok; VJP, Vajepar; KNM, Kanmer; BHA, Bhachau; BEL, Bela; GDD, Gadhada; JUM, Jumkunaria; MTP, Motapaya; NGR, Nagor; BHU, Bhuj; NPR, Narayanpar; TPM, Tapar Mundra; MND, Mandvi; VGH, Vaghura; TPR, Tapar Anjar; NDD, New Dudhai; KVD, Kavada; VND, Vondh; KNP, Khingarpar; and GDM, Gandhidham). The average Indian plate velocity of 54 mm/year in NE direction is shown by a lack arrow. The inset shows the key map for the area, where the study area is shown by an open square. A black arrow shows the prevailing compression direction over the Indian continent. (b) Epicentral plot of 241 teleseismic events, whose broadband data are used for our RF study. The filled red triangle symbol marks the centre of our network (latitude 70^{o}E, longitude 23^{o}N) while filled green diamond symbols mark epicentres of selected teleseismic events.

Figure 2: A plot showing Bouguer gravity anomaly (in mGals) map of Kachchh, Gujarat (after Mishra et al., 2005; Tewari et al., 2009; Khan et al., 2017). Solid red large filled circles show locations of moderate to large earthquakes in Kachchh, Gujarat (viz. 1819 M_w7.8 Allah-Bund, 1956 M_w6.0 Anjar, 2001 M_w7.7 Bhuj and 2006 M_w5.6 Gedi Events). BU=Bela uplift, GF=Gedi Fault, KHF=Katrol Hill Fault, KMF = Kachchh Mainland Fault, KU= Khadir uplift, KWU = Kathiawar uplift, PU = Pachham uplift, SWF = SouthWagad Fault, VGF = Vigodi Fault, and WU=Wagad uplift. (a) Black circles represent Joint Hypocentral Determination (JHD) relocations of aftershocks during 2001-06, (b) black circles represent JHD relocations of aftershocks during 2007-08, and (c) black circles represent JHD relocations of aftershocks during 2009-2016.

Figure 3: Individual radial P-receiver functions stored according to their back-azimuths, which have been estimated for a Gaussian width (a) = 2.5, at different stations in Kachchh (a) JUM, (b) GDM, (c) KNP, (d) MTP, (e) NDD, (f) TPR, (g) BHU, (h) VND, (i) VJP, (j) BHA, (k) NPR, (l) TPM, (m) GDD, (n) BEL, and (o) NGR. On the top of every figure stacked P-RF corresponding to each station is also shown.

Figure 4: (a) Ray coverage of the surface-wave group velocity dispersion study. Open blue squares mark the stations, whereas red open circles represent the epicenters of the considered 8 events for the study. (b) Average stacked fundamental mode Rayleigh-wave group velocity dispersion curves versus time period, and (c) average stacked fundamental mode Love-wave group velocity dispersion curves versus time period. Error bars show standard deviations.

Figure 5.Good agreement between observed (black line) and inverted (red line) radial RFs with a=1.0 and 2.5, for different horizontal slowness (s, in s/km), obtained through joint inversion of P-RFs and group velocity dispersion data of Rayleigh and Love waves at different stations, (a) BHA, (b) JUM, (c) BEL, and (d) BHU. Date marks the year, month and day of the teleseismic event, whose data is used for RF study. "a" and "R%" represent gaussian width factor (used for estimating RF) and agreement (in %) between observed and inverted RFs, respectively, while S(s/km) represents the horizontal slowness.

Figure 6.Same as Fig. 5 for stations (a) GDD, (b) MTP, (c) KVD, and (d) NGR.

Figure 7. Same as Fig. 5 for stations (a) KNM, (b) NPR, (c) MND, and (d) VND.

Figure 8. Same as Fig. 5 for stations (a) TPM, (b) SIV, (c) NDD, and (d) TPR.

Figure 9. Same as Fig. 5 for stations (a) KNP, (b) VJP, (c) VGH, and (d) GDM.

Figure 10. inverted shear velocity models showing Moho (M) and LAB (L) depth estimates, which are obtained through joint inversion of P-RFs and group velocity dispersion data of Rayleigh and Love waves at different stations, (a) BHA, (b) BEL, (c) JUM, (d) BHU, (e) GDD, and (f) MTP. Different colors represent different Vs models used for the RF inversion.

Figure 11.Same as Fig. 10 for stations (a) KVD, (b) NGR, (c) KNM, (d) NPR, (e) MND, and (f) VND.

Figure 12.Same as Fig. 10 for stations (a) NDD, (b) SIV, (c) TPM, (d) TPR, (e) KNP, and (f) VJP.

Figure 13. (a) Inverted shear velocity models showing Moho (M) and LAB (L) depth estimates, which are obtained through joint inversion of P-RFs and group velocity dispersion data of Rayleigh and Love waves at (a) VGH and (b) GDM stations. (c) Modeled crustal thickness (in km) map of the Kachchh region, and (d) Modeled Lithospheric thickness (in km) map of the Kachchh region. Red open circles mark negative travel-time residuals and black open circles show positive travel-time residuals.Filled brown triangles mark broadband seismograph stations in Kachchh, Gujarat. Major tectonic faults in Kachchh are marked by solid red lines.

Figure 14: (a) Residual Bouguer gravity anomaly map reconstructed using high-pass filter, with cut-off wavelength of 375 km. (after Khan et al 2017). Grey open circles mark the Joint Hypocentral Determination (JHD) relocations of aftershocks of the 2001 Bhuj mainshock, during 2001-06. Faults are marked be red lines. AB section marked be solid blue line shows the extent of the Samkhiali graben (from KMF to NWF), where most of the seismicity is found to be confined during 2001-06, extending from 2 to 35 km depth. (b) NE trending tectonic cross-section showing major tectonic features (like uplift, graben and faults) in the Kachchh region.

The black thick lines mark the modelled Moho and LAB depths, from the present study. Large solid red circle marks the hypocenter of the 2001 Bhuj mainshock while open red circles mark the selected M5 aftershocks of the 2001 Bhuj earthquake, during 2001-06.

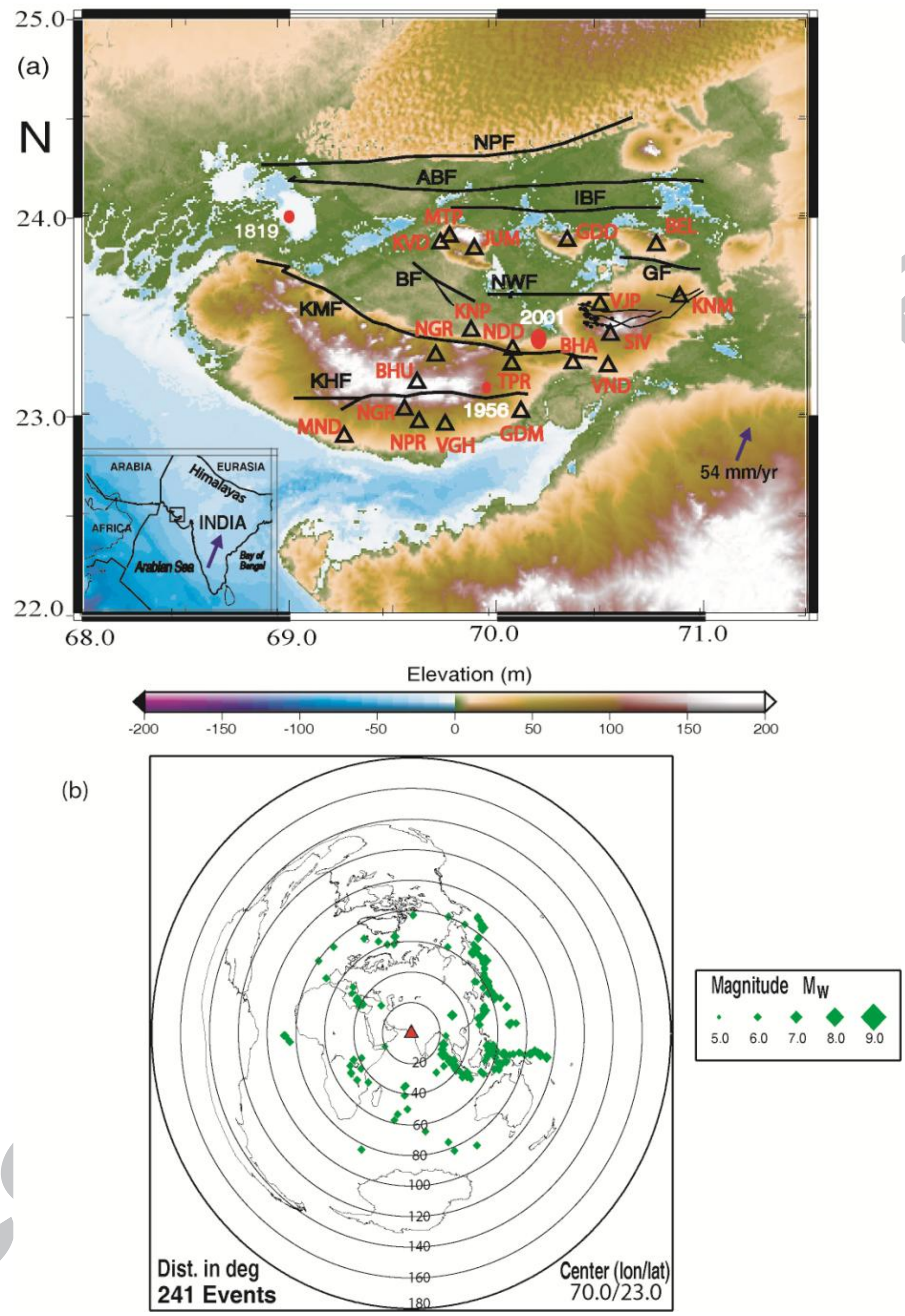

Figure 1. (a) Elevation (in m) map showing station distribution in Kachchh, Gujarat. Open black triangles mark the broadband seismograph stations (SIV, Sivlok; VJP, Vajepar; KNM, Kanmer; BHA, Bhachau; BEL, Bela; GDD, Gadhada; JUM, Jumkunaria; MTP, Motapaya; NGR, Nagor; BHU, Bhuj; NPR, Narayanpar; TPM, Tapar Mundra; MND, Mandvi; VGH, Vaghura; TPR, Tapar Anjar; NDD, New Dudhai; KVD, Kavada; VND, Vondh; KNP, Khingarpar; and GDM, Gandhidham). The average Indian plate velocity of 54 mm/year in NE direction is shown by a

lack arrow. The inset shows the key map for the area, where the study area is shown by an open square. A black arrow shows the prevailing compression direction over the Indian continent. (b) Epicentral plot of 241 teleseismic events, whose broadband data are used for our RF study. The filled red triangle symbol marks the centre of our network (latitude 70^{o}E, longitude 23^{o}N) while filled green diamond symbols mark epicentres of selected teleseismic events.

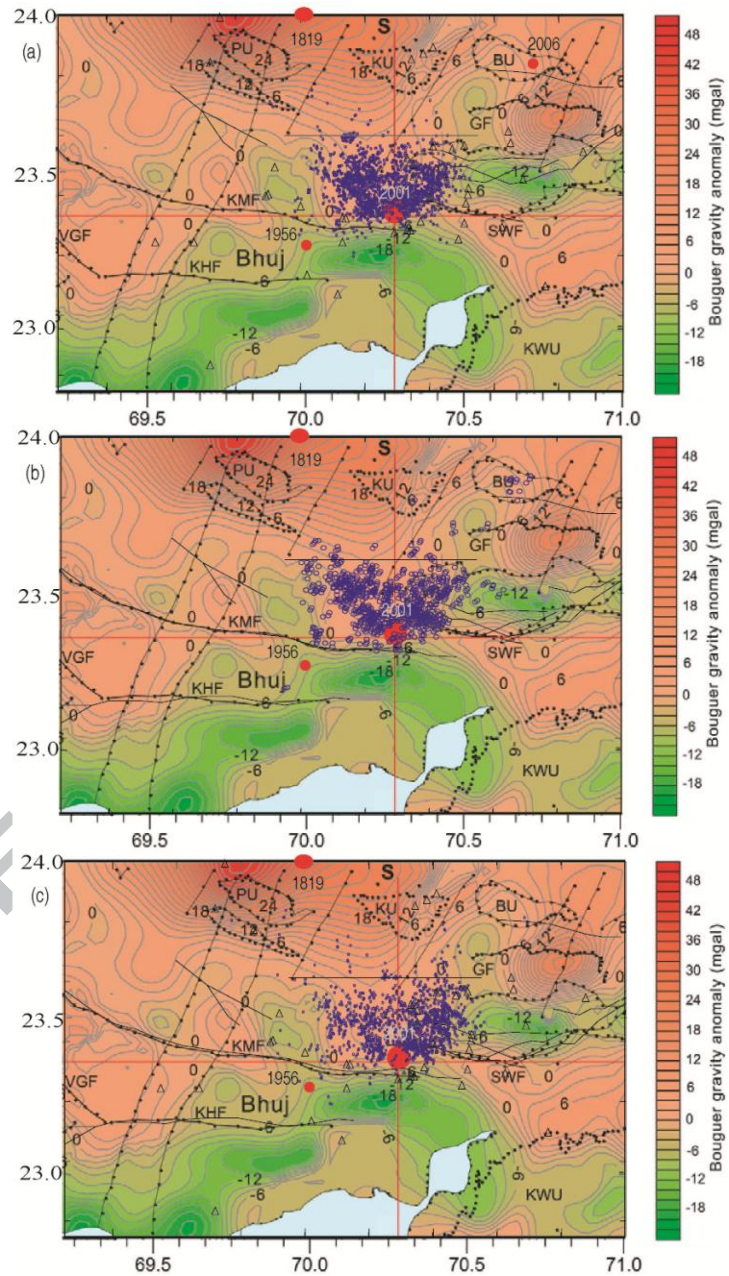

Figure 2: A plot showing Bouguer gravity anomaly (in mGals) map of Kachchh, Gujarat (after Mishra et al., 2005; Tewari et al., 2009; Khan et al., 2017). Solid red large filled circles show locations of moderate to large earthquakes in Kachchh, Gujarat (viz. 1819 M_w7.8 Allah-Bund, 1956 M_w6.0 Anjar, 2001 M_w7.7 Bhuj and 2006 M_w5.6 Gedi Events). BU=Bela uplift, GF=Gedi Fault, KHF=Katrol Hill Fault, KMF = Kachchh Mainland Fault, KU= Khadir uplift, KWU = Kathiawar uplift, PU = Pachham uplift, SWF = SouthWagad Fault, VGF = Vigodi Fault, andWU=Wagad uplift. (a) black circles represent JHD relocations of aftershocks during 2001-06, (b) black circles represent JHD relocations of aftershocks during 2007-08, and (c) black circles represent JHD relocations of aftershocks during 2009-2016.

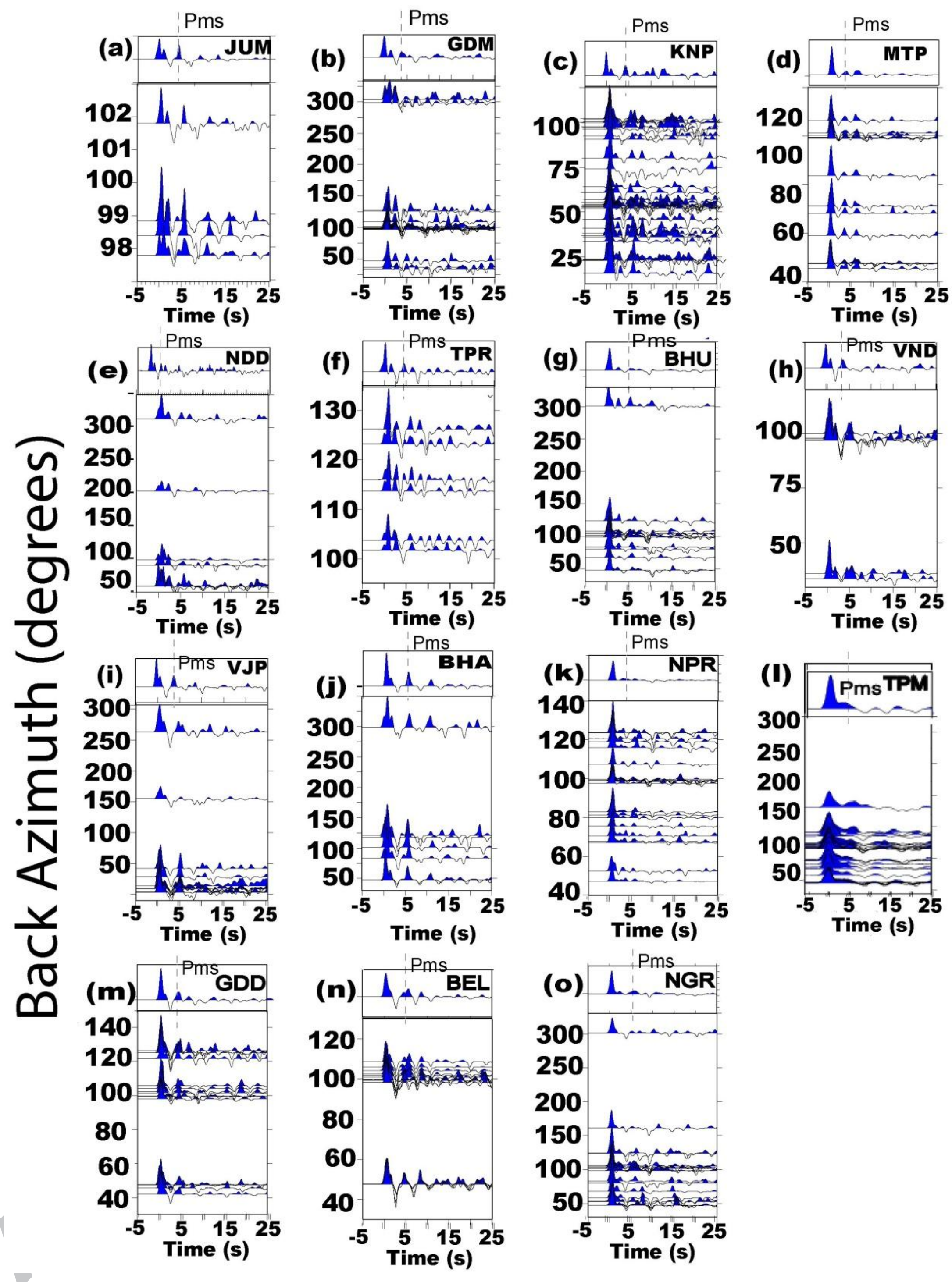

Figure 3. Individual radial P-receiver functions stored according to their back-azimuths, which have been estimated for a Gaussian width (a) = 2.5, at different stations in Kachchh (a) JUM, (b) GDM, (c) KNP, (d) MTP, (e) NDD, (f) TPR, (g) BHU, (h) VND, (i) VJP, (j) BHA, (k) NPR, (l)

TPM, (m) GDD, (n) BEL, and (o) NGR. On the top of every figure stacked P-RF corresponding to each station is also shown.

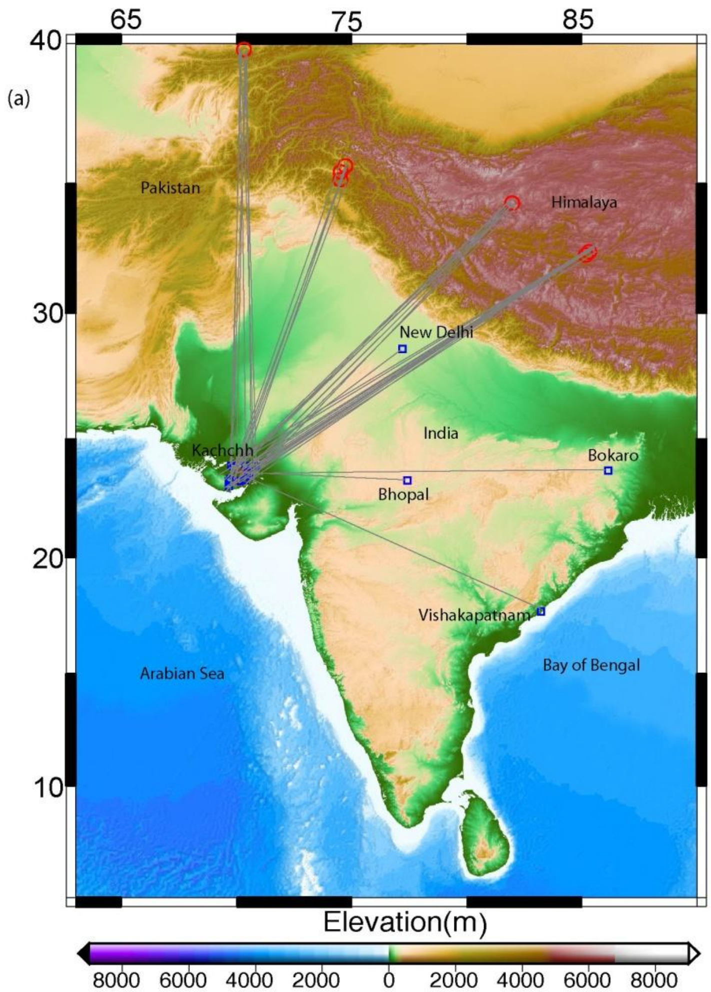

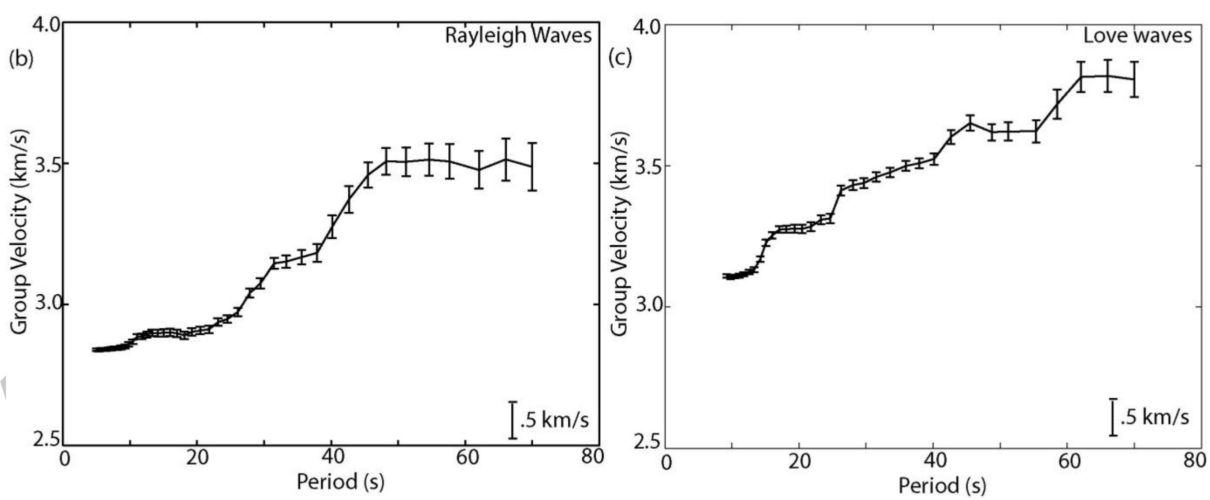

Figure 4: (a) Ray coverage of the surface-wave group velocity dispersion study. Open blue squares mark the stations, whereas red open circles represent the epicenters of the considered 8 events for the study. (b) average stacked fundamental mode Rayleigh-wave group velocity

dispersion curves versus time period, and (c) average stacked fundamental mode Love-wave group velocity dispersion curves versus time period. Error bars show standard deviations.

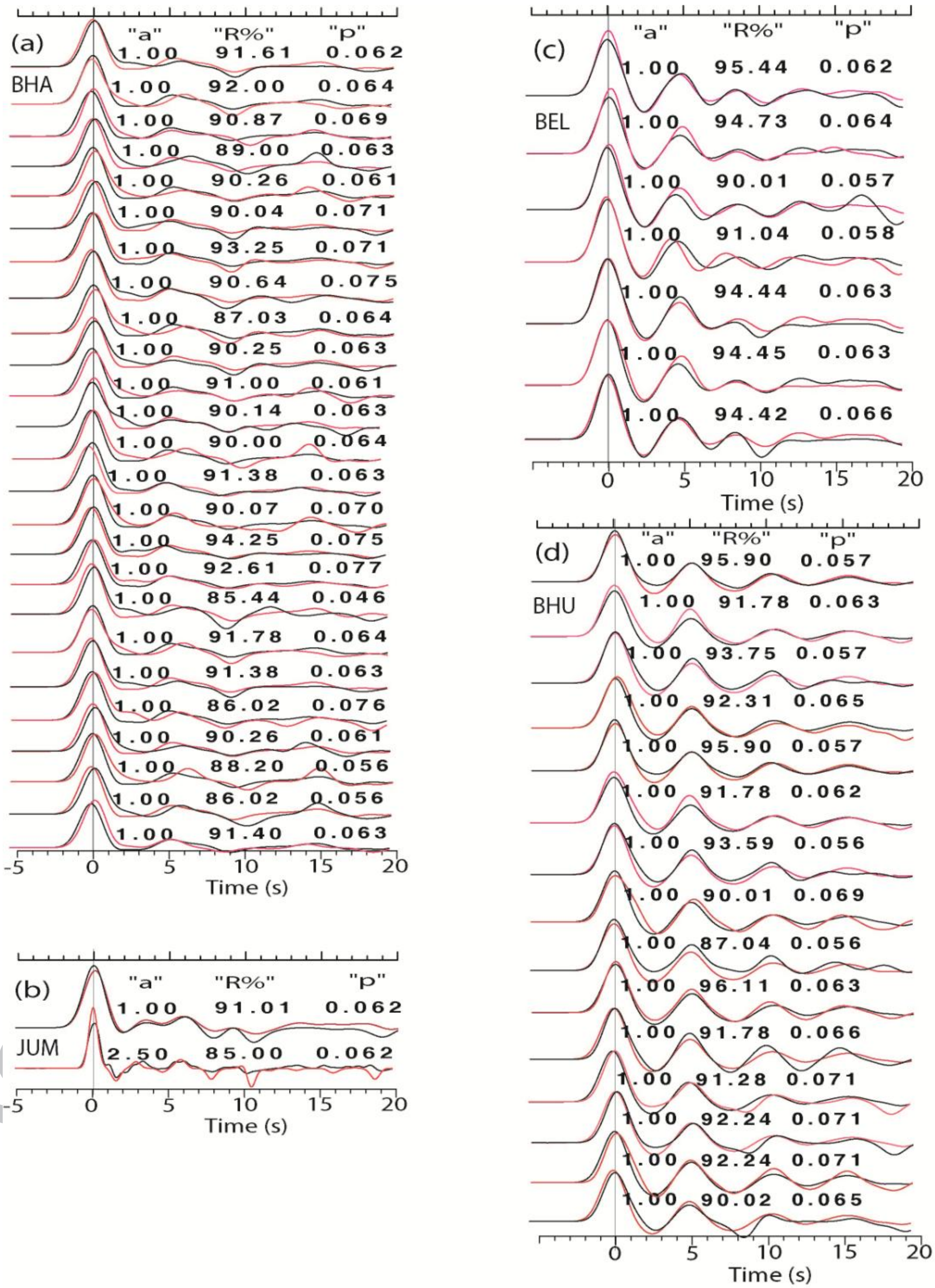

Figure 5. Good agreement between observed (black line) and inverted (red line) radial RFs with a=1.0 and 2.5, for different horizontal slowness (s, in s/km), obtained through joint inversion of P-RFs and group velocity dispersion data of Rayleigh and Love waves at different stations, (a) BHA, (b) JUM, (c) BEL, and (d) BHU. Date marks the year, month and day of the teleseismic event, whose data is used for RF study. "a" and "R%" represent gaussian width factor (used for estimating RF) and agreement (in %) between observed and inverted RFs, respectively, while S(s/km) represents the horizontal slowness.

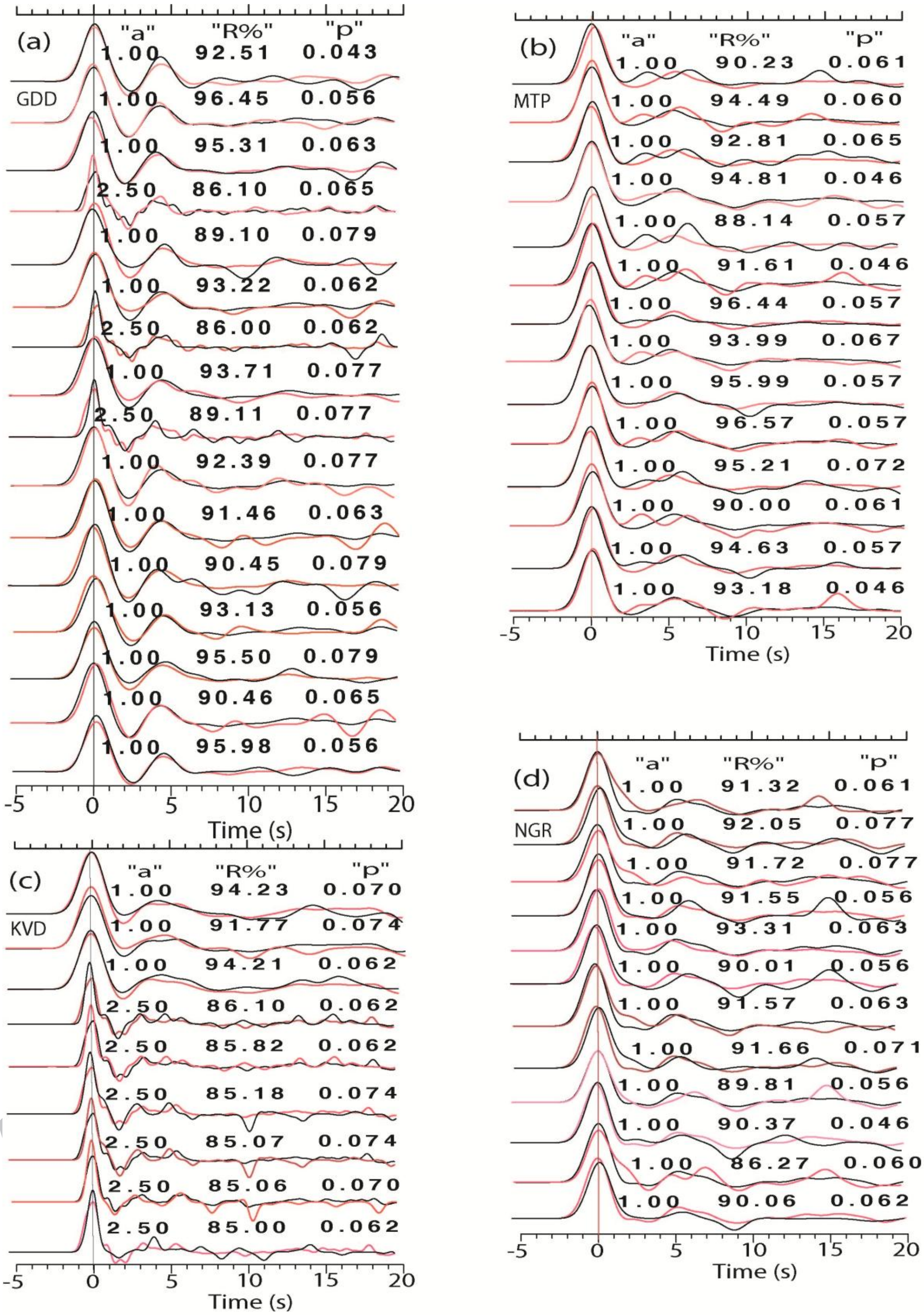
(a)
GDD
"a" "R%" "p"
1.00 92.51 0.043
1.00 96.45 0.056
1.00 95.31 0.063
2.50 86.10 0.065
1.00 89.10 0.079
1.00 93.22 0.062
2.50 86.00 0.062
1.00 93.71 0.077
2.50 89.11 0.077
1.00 92.39 0.077
1.00 91.46 0.063
1.00 90.45 0.079
1.00 93.13 0.056
1.00 95.50 0.079
1.00 90.46 0.065
1.00 95.98 0.056
-5 0 5 10 15 20
Time (s)
(b)
MTP
"a" "R%" "p"
1.00 90.23 0.061
1.00 94.49 0.060
1.00 92.81 0.065
1.00 94.81 0.046
1.00 88.14 0.057
1.00 91.61 0.046
1.00 96.44 0.057
1.00 93.99 0.067
1.00 95.99 0.057
1.00 96.57 0.057
1.00 95.21 0.072
1.00 90.00 0.061
1.00 94.63 0.057
1.00 93.18 0.046
-5 0 5 10 15 20
Time (s)
(c)
KVD
"a" "R%" "p"
1.00 94.23 0.070
1.00 91.77 0.074
1.00 94.21 0.062
2.50 86.10 0.062
2.50 85.82 0.062
2.50 85.18 0.074
2.50 85.07 0.074
2.50 85.06 0.070
2.50 85.00 0.062
-5 0 5 10 15 20
Time (s)
(d)
NGR
"a" "R%" "p"
1.00 91.32 0.061
1.00 92.05 0.077
1.00 91.72 0.077
1.00 91.55 0.056
1.00 93.31 0.063
1.00 90.01 0.056
1.00 91.57 0.063
1.00 91.66 0.071
1.00 89.81 0.056
1.00 90.37 0.046
1.00 86.27 0.060
1.00 90.06 0.062
-5 0 5 10 15 20
Time (s)

Figure 6. Same as Fig. 5 for stations (a) GDD, (b) MTP, (c) KVD, and (d) NGR.

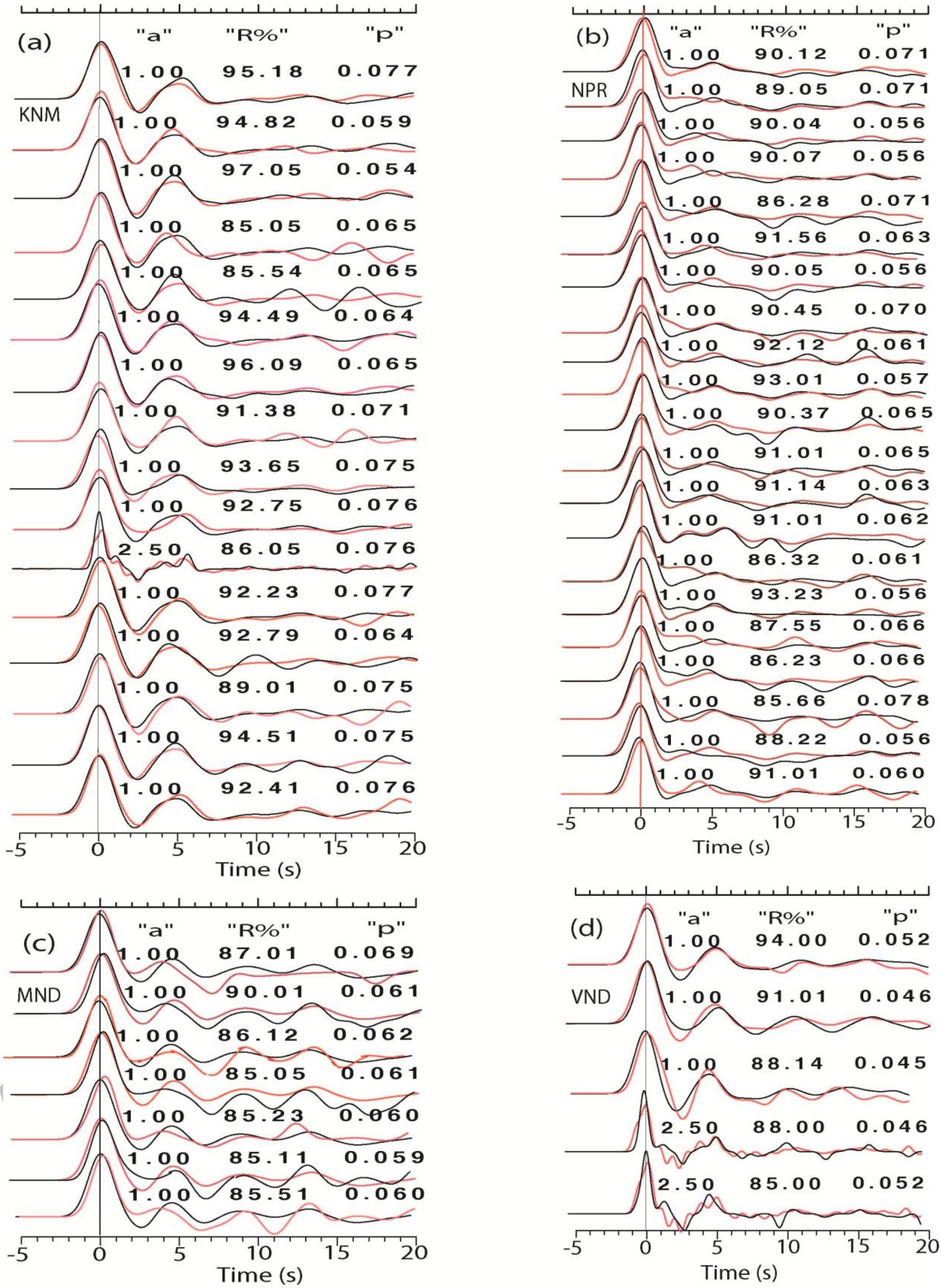
(a)
"a" "R%" "p"
KNM
1.00 95.18 0.077
1.00 94.82 0.059
1.00 97.05 0.054
1.00 85.05 0.065
1.00 85.54 0.065
1.00 94.49 0.064
1.00 96.09 0.065
1.00 91.38 0.071
1.00 93.65 0.075
1.00 92.75 0.076
2.50 86.05 0.076
1.00 92.23 0.077
1.00 92.79 0.064
1.00 89.01 0.075
1.00 94.51 0.075
1.00 92.41 0.076
-5 0 5 10 15 20
Time (s)
(b)
"a" "R%" "p"
NPR
1.00 90.12 0.071
1.00 89.05 0.071
1.00 90.04 0.056
1.00 90.07 0.056
1.00 86.28 0.071
1.00 91.56 0.063
1.00 90.05 0.056
1.00 90.45 0.070
1.00 92.12 0.061
1.00 93.01 0.057
1.00 90.37 0.065
1.00 91.01 0.065
1.00 91.14 0.063
1.00 91.01 0.062
1.00 86.32 0.061
1.00 93.23 0.056
1.00 87.55 0.066
1.00 86.23 0.066
1.00 85.66 0.078
1.00 88.22 0.056
1.00 91.01 0.060
-5 0 5 10 15 20
Time (s)
(c)
"a" "R%" "p"
MND
1.00 87.01 0.069
1.00 90.01 0.061
1.00 86.12 0.062
1.00 85.05 0.061
1.00 85.23 0.060
1.00 85.11 0.059
1.00 85.51 0.060
-5 0 5 10 15 20
Time (s)
(d)
"a" "R%" "p"
VND
1.00 94.00 0.052
1.00 91.01 0.046
1.00 88.14 0.045
2.50 88.00 0.046
2.50 85.00 0.052
-5 0 5 10 15 20
Time (s)

Figure 7. Same as Fig. 5 for stations (a) KNM, (b) NPR, (c) MND, and (d) VND.

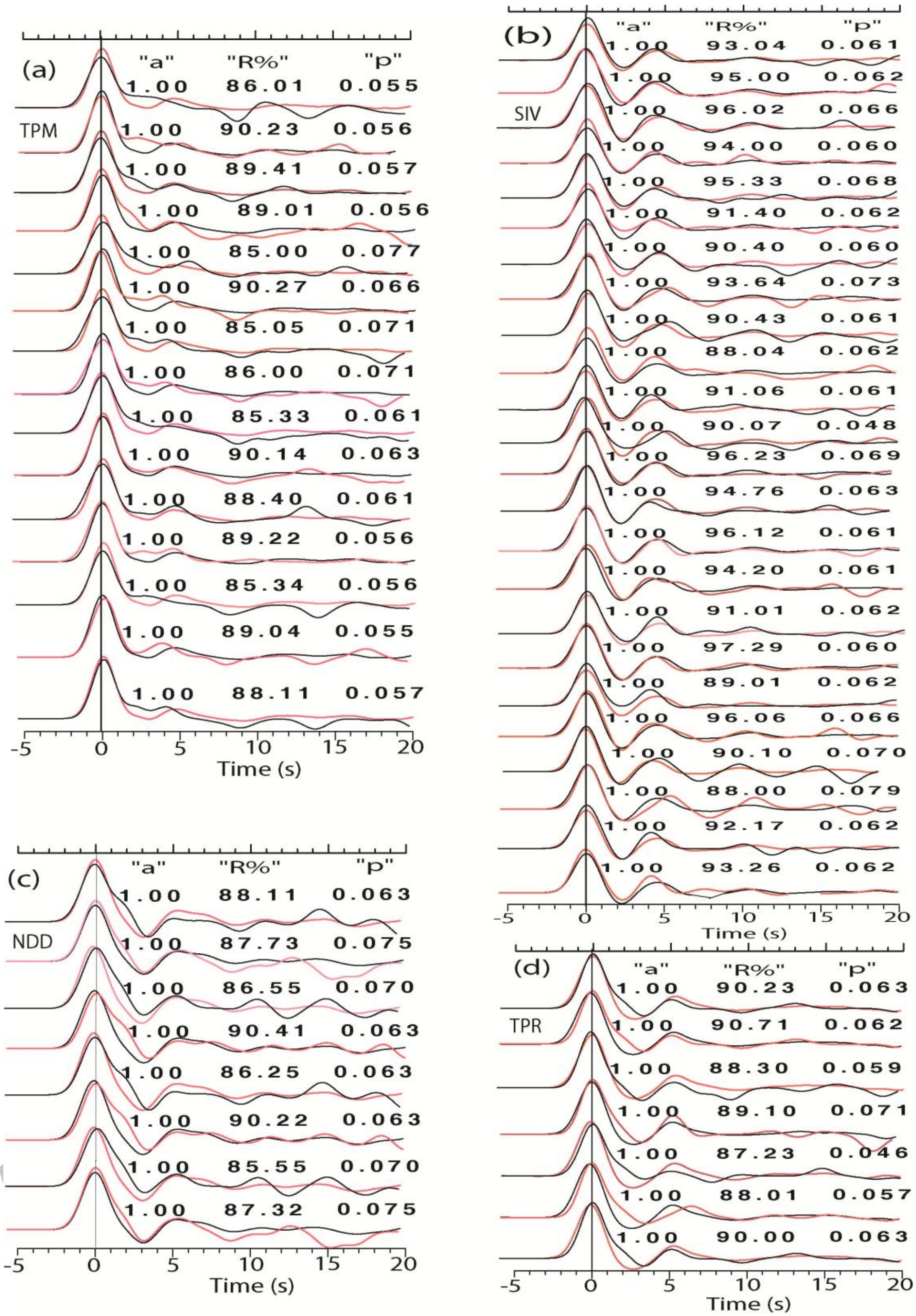

Figure 8. Same as Fig. 5 for stations (a) TPM, (b) SIV, (c) NDD, and (d) TPR.

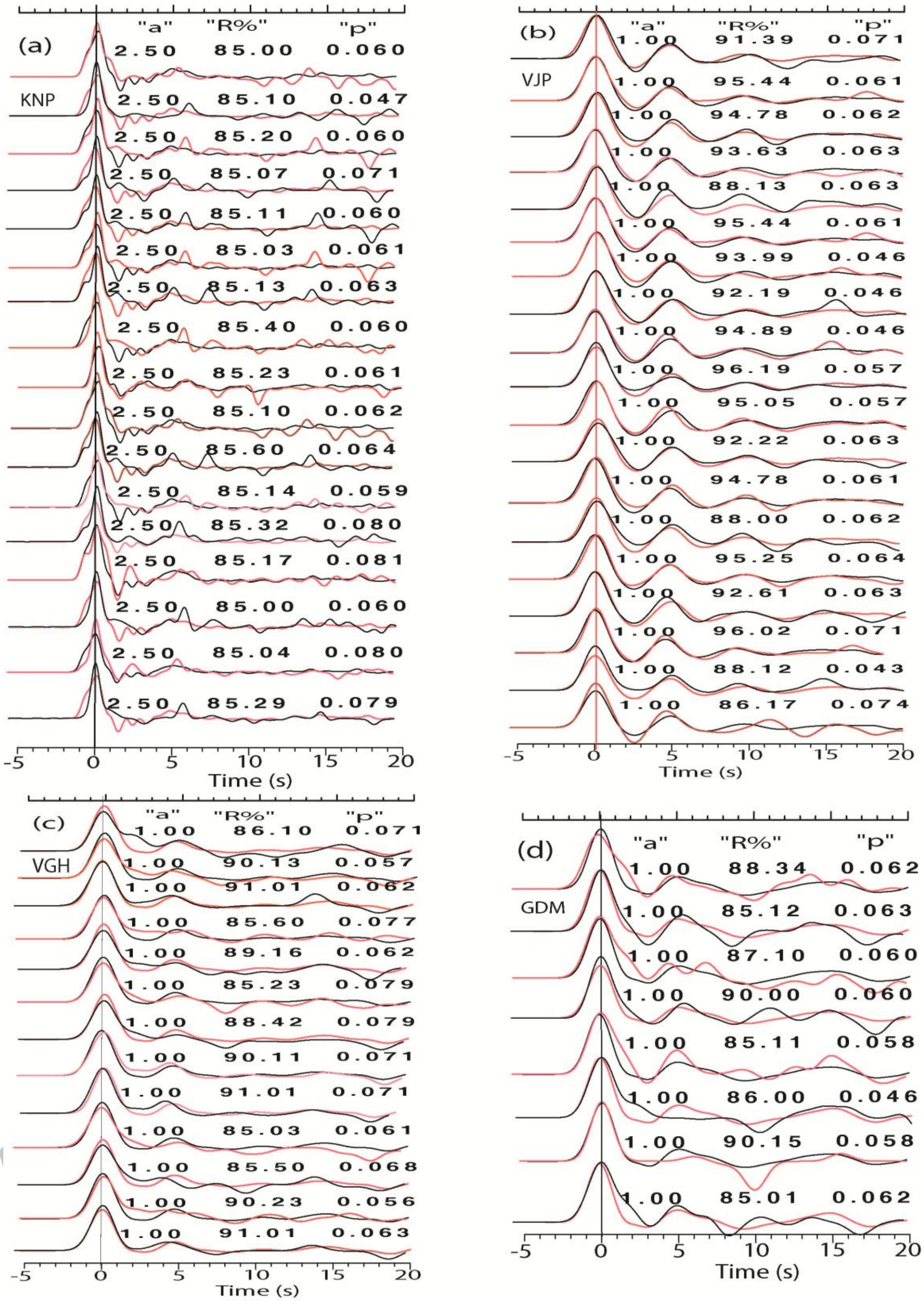

Figure 9. Same as Fig. 5 for stations (a) KNP, (b) VJP, (c) VGH, and (d) GDM.

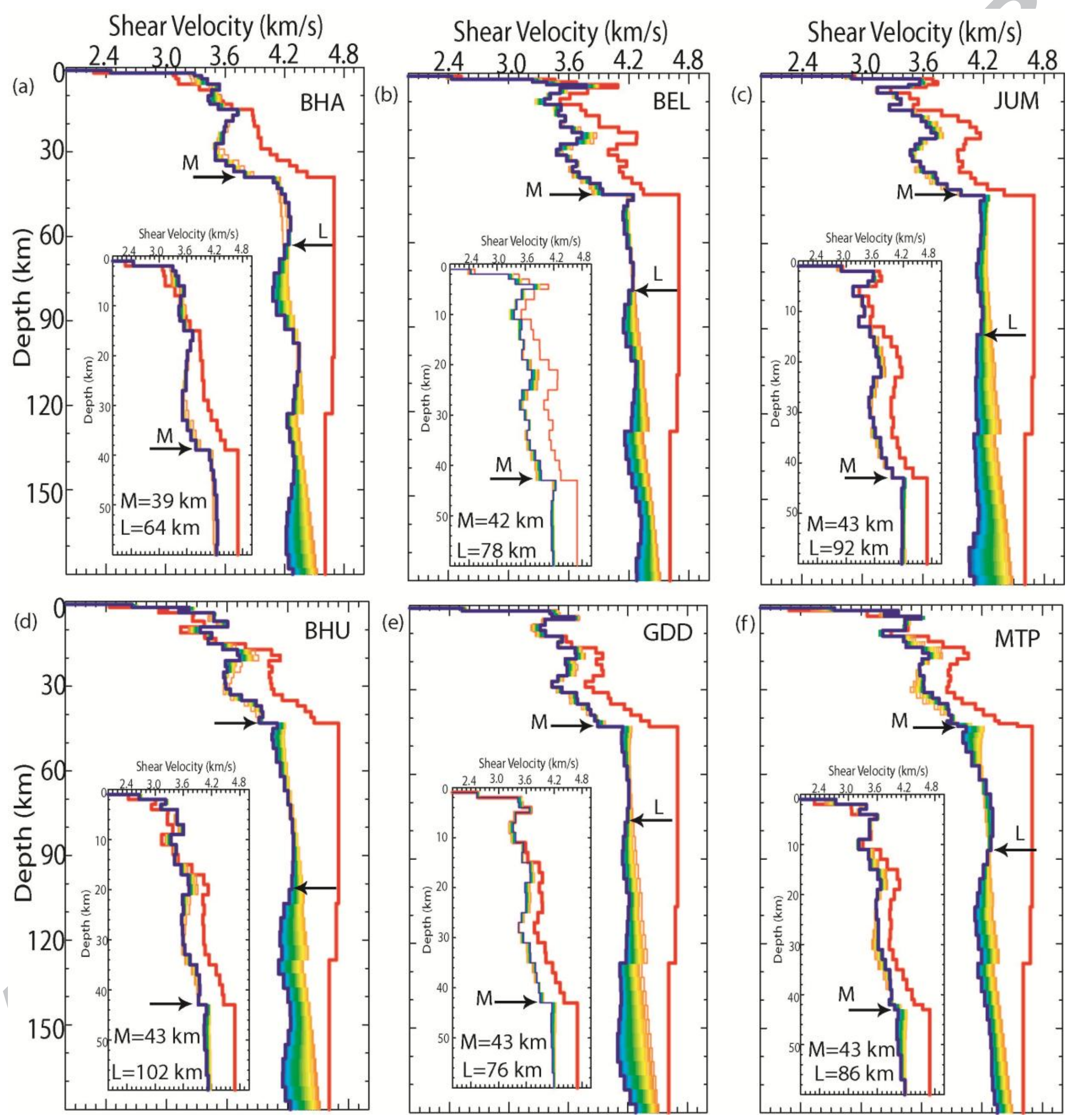

Figure 10. inverted shear velocity models showing Moho (M) and LAB (L) depth estimates, which are obtained through joint inversion of P-RFs and group velocity dispersion data of

Rayleigh and Love waves at different stations, (a) BHA, (b) BEL, (c) JUM, (d) BHU, (e) GDD, and (f) MTP. Different colors represent different Vs models used for the RF inversion.

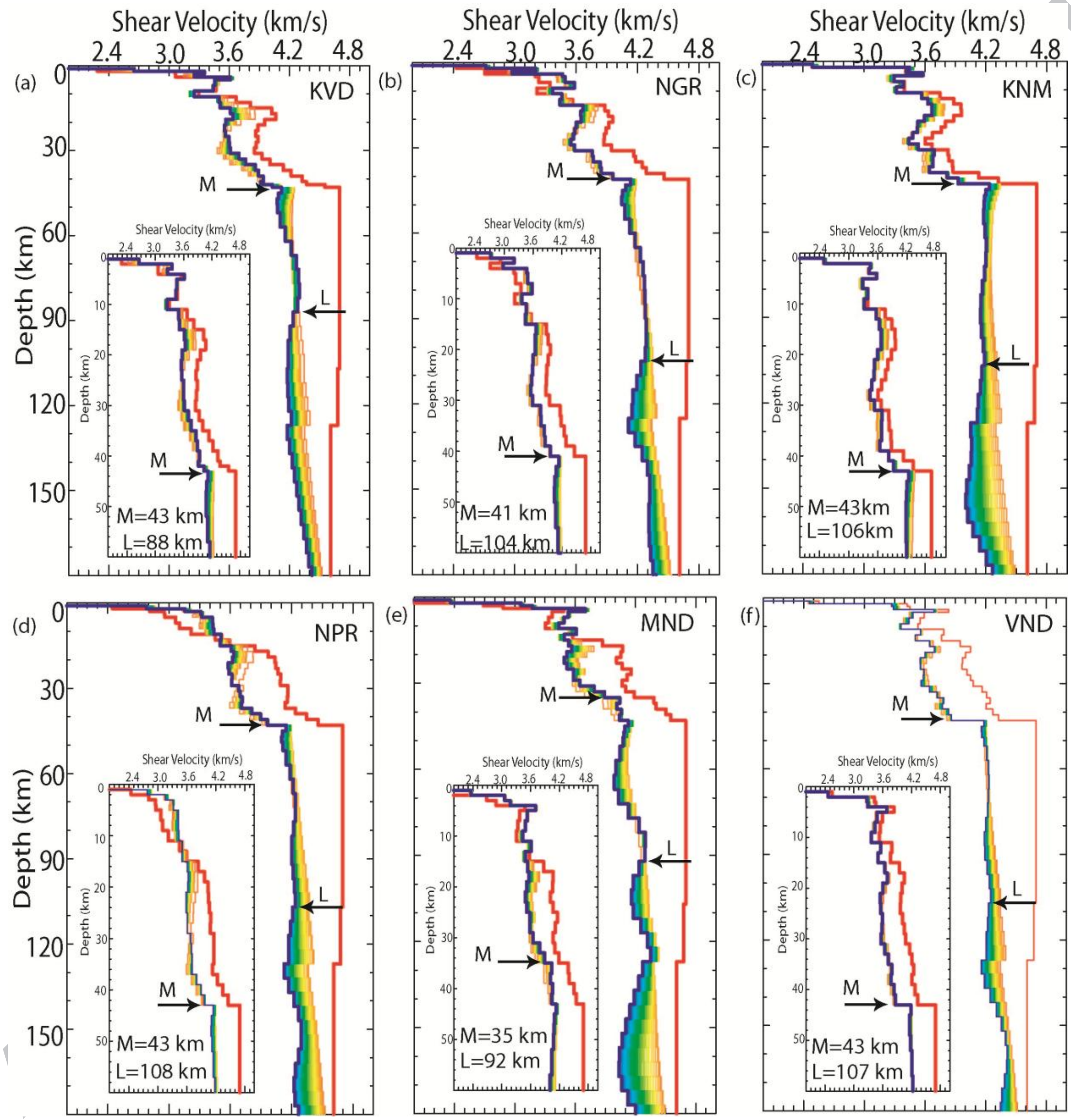

Figure 11. Same as Fig. 11 for stations (a) KVD, (b) NGR, (c) KNM, (d) NPR, (e) MND, and (f) VND.

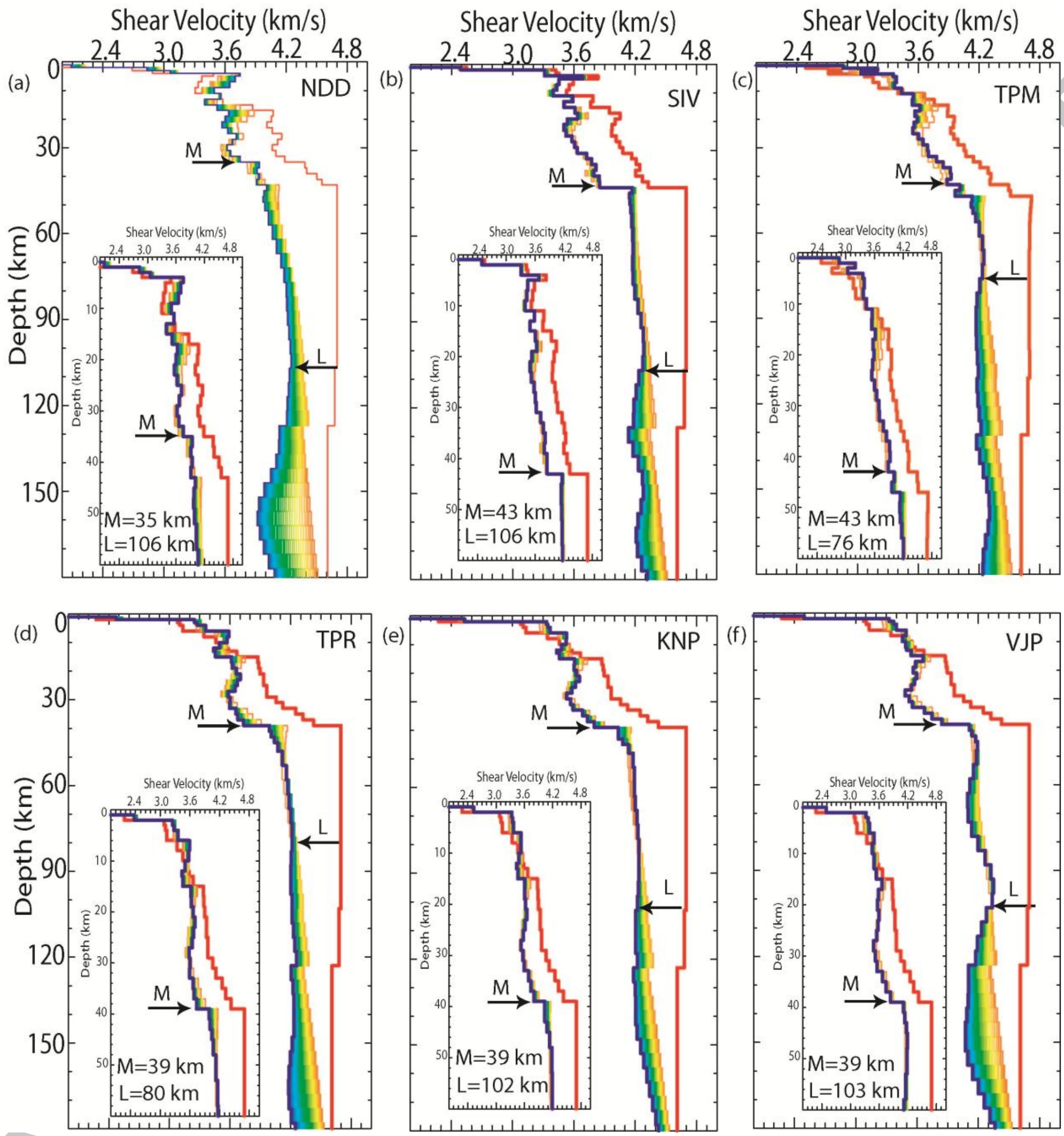

Figure 12. Same as Fig. 11 for stations (a) NDD, (b) SIV, (c) TPM, (d) TPR, (e) KNP, and (f) VJP.

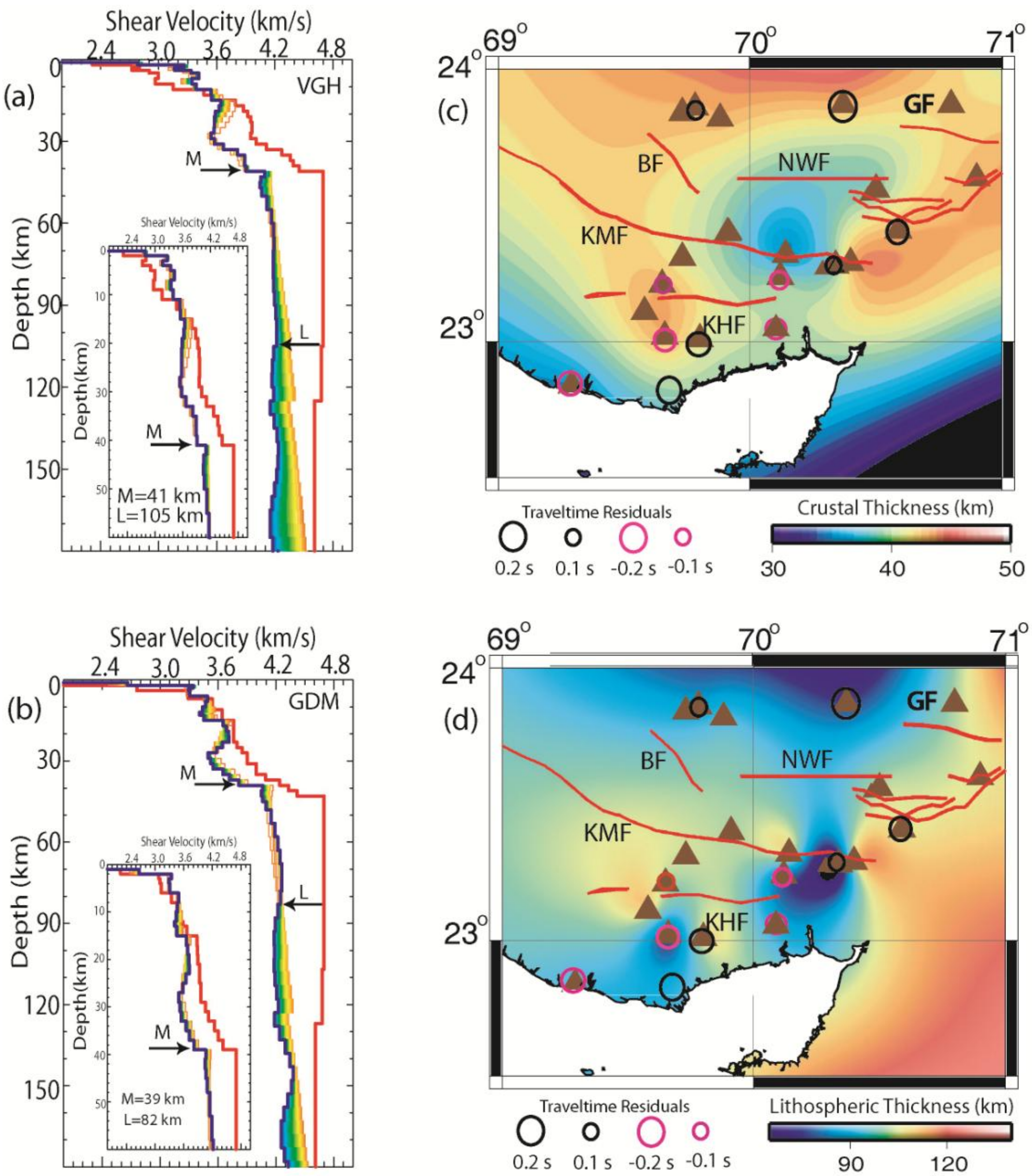

Figure 13. (a) Inverted shear velocity models showing Moho (M) and LAB (L) depth estimates, which are obtained through joint inversion of P-RFs and group velocity dispersion data of Rayleigh and Love waves at (a) VGH and (b) GDM stations. (c) Modeled crustal thickness (in km) map of the Kachchh region, and (d) Modeled Lithospheric thickness (in km) map of the Kachchh region. Red open circles mark negative travel-time residuals and black open circles show positive travel-time residuals. Filled brown triangles mark broadband seismograph stations in Kachchh, Gujarat. Major tectonic faults in Kachchh are marked by solid red lines.

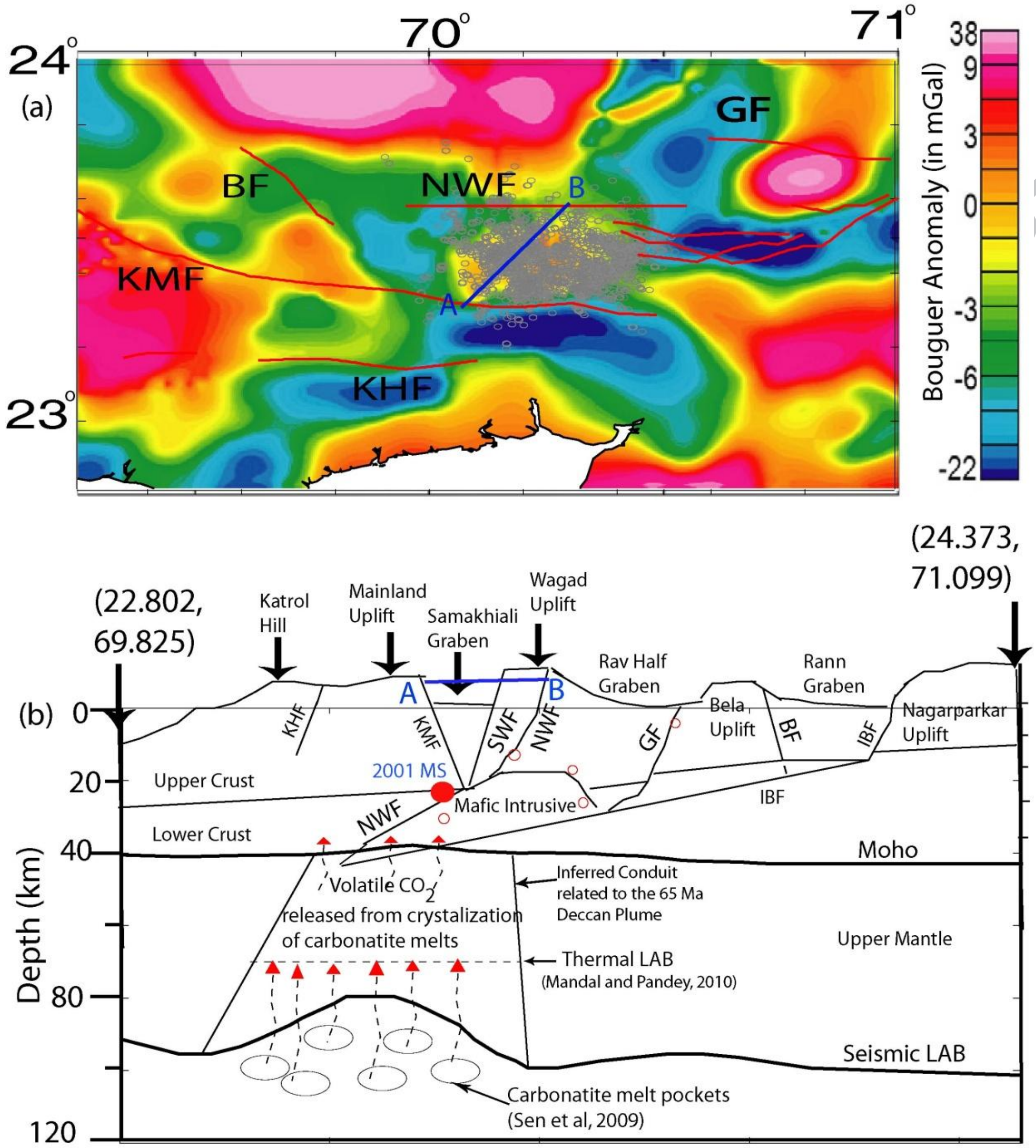

Figure 14: (a) Residual Bouguer gravity anomaly map reconstructed using high-pass filter, with cutoff wavelength of 375 km. (after Khan et al 2017). Grey open circles mark the JHD relocations of aftershocks of the 2001 Bhuj mainshock, during 2001-06. Faults are marked be red lines. AB section marked be solid blue line shows the extent of the Samkhiali graben (from KMF to NWF), where most of the seismicity is found to be confined during 2001-06, extending from 2 to 35 km depth. (b) NE trending tectonic cross-section showing major tectonic features (like uplift, graben and faults) in the Kachchh region. The black thick lines mark the modelled Moho and LAB depths, from the present study. Large solid red circle marks the hypocenter of the 2001

Bhuj mainshock while open red circles mark the selected M5 aftershocks of the 2001 Bhuj earthquake, during 2001-06.

Table 1: Estimated depths of Moho and lithosphere-asthenosphere boundary(LAB)below Kachchh, Gujarat

S. N.	Stn. name	Lat. (N)	Lon. (E)	Moho Depth (km)	Mean Moho Depth (km)	LAB Thick (km)	Mean Lab Thick (km)	Drop in Vs(%) across LAB	Mean drop in Vs (%)
Samkhiali Graben / Central Kachchh Rift Zone (CKRZ)									
1	KNP	23.40	69.91	39	38 ± 2	92	88±16	2.4	4.0 ± 1.3
2	BHA	23.28	70.34	39		64		3.5	
3	TPR	23.24	70.12	39		80		4.0	
4	VJP	23.56	70.50	39		103		5.0	
5	GDM	23.06	70.11	39		82		3.0	
6	NDD	23.32	70.14	35		106		5.8	
EAST OF CKRZ (surrounding un-rifted zone)									
7	VND	23.29	70.40	43	43	72	85±18	2.2	3.7 ± 1.7
8	SIV	23.41	70.59	43		106		3.5	
9	KNM	23.60	70.90	43		78		5.5	
NORTH OF CKRZ (surrounding un-rifted zone)									
10	BEL	23.87	70.80	42	43±1	78	84±7	4.8	4.3 ± 0.7
11	GDD	23.87	70.37	43		76		4.8	
12	JUM	23.82	69.88	43		92		4.8	
13	KVD	23.84	69.73	43		88		3.5	
14	MTP	23.86	69.78	43		86		3.5	
SOUTH-WEST OF CKRZ (surrounding un-rifted zone)									
15	BHU	23.21	69.65	43		102		4.8	4.0

16	NGR	23.31	69.73	41	42±1	104	93±15	4.8	±0.7
17	NPR	23.11	69.58	43		77		3.5	
18	TPM	23.02	69.66	43		76		3.5	
19	VGH	23.01	69.80	41		106		3.6	
COASTAL STATION IN THE SOUTH-WEST OF CKRZ									
20	MND	22.84	69.29	35	35	103	103	7.2	7.2

Graphical abstract

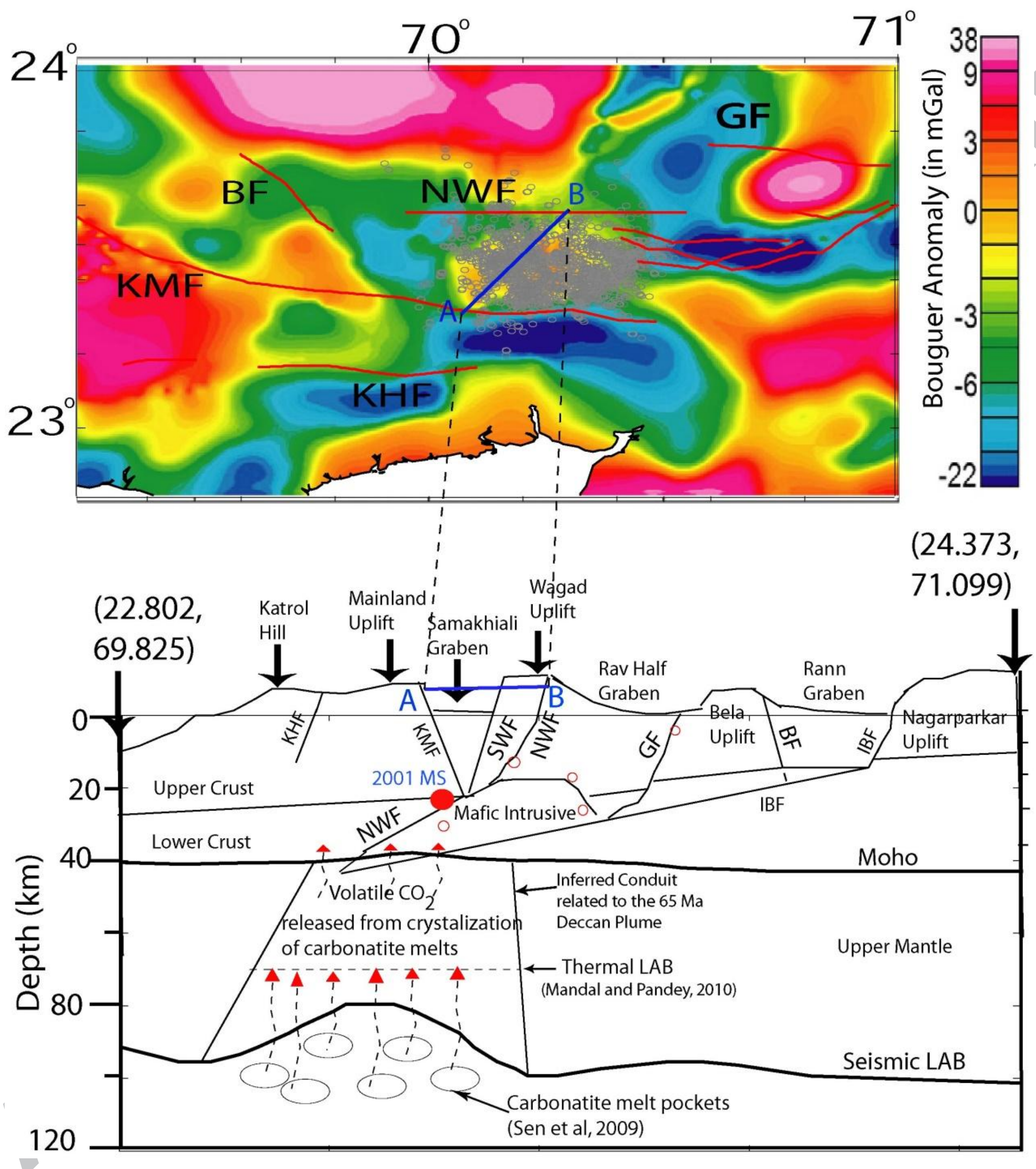

Highlights

- Estimated crustal and lithospheric thicknesses in Kachchh range from 35 to 43 km and 64 to 106 km, respectively
- The Samkhiali graben (SG) is characterized by a marked crustal and lithospheric thinning.
- Such a local tectonic setup along with the N-S compression of Indian plate can lead to a stress regime associated with the SG near to critical
- Entrapped volatile CO_2 and metamorphic fluids provide the required triggering mechanism to generate earthquakes within the SG